NACA

RESEARCH MEMORANDUM

EFFECT OF VARIATIONS IN REYNOLDS NUMBER ON THE

AERODYNAMIC CHARACTERISTICS OF THREE BOMB

OR STORE SHAPES AT A MACH NUMBER

OF 1.62 WITH AND WITHOUT FINS

By Robert W. Rainey

Langley Aeronautical Laboratory
Langley Field, Va.

NATIONAL ADVISORY COMMITTEE
FOR AERONAUTICS
WASHINGTON

June 25, 1953
Declassified April 8, 1957

NATIONAL ADVISORY COMMITTEE FOR AERONAUTICS

———

RESEARCH MEMORANDUM

———

EFFECT OF VARIATIONS IN REYNOLDS NUMBER ON THE

AERODYNAMIC CHARACTERISTICS OF THREE BOMB

OR STORE SHAPES AT A MACH NUMBER

OF 1.62 WITH AND WITHOUT FINS

By Robert W. Rainey

SUMMARY

Tests have been made in the Langley 9-inch supersonic tunnel of three bomb or store shapes without fins and with two sets of cruciform fins. These investigations were made at a Mach number of 1.62 at Reynolds numbers from 0.40×10^6 to 9.70×10^6, based on the closed body lengths. The maximum angle-of-attack range was from -4° to 10°. Measurements of normal force, chord force, and pitching moment were made; analyses of the effects of angle of attack and Reynolds number upon these quantities and also upon center-of-pressure position and fin effectiveness are presented.

The results indicated that the configurations having a fineness ratio of 8.6 with small fins and the configurations having fineness ratios of 5, 7, and 8.6 with large fins were statically stable about a typical center-of-gravity position at 45 percent of the closed body length at all angles of attack and at all test Reynolds numbers. Also, the results showed that it is possible to design a supersonic bomb or store configuration having a constant change in normal-force coefficient with angle of attack or center-of-pressure position or both for angles of attack near 0° and for Reynolds numbers of the order of 3×10^6 and greater.

INTRODUCTION

One of the problems that is associated with the development of supersonic service aircraft is the proper design of either the bombs or stores, or both, that may be carried by the aircraft. In such design, consideration must be given to the aerodynamic characteristics of the

isolated bombs or stores. These characteristics are important in the
determination of the mutual interference effects of an externally mounted
bomb or store and the aircraft, as well as in the determination of the
breakaway characteristics and trajectories of bombs whether released
from internal, semiexternal, or external locations.

When static wind-tunnel tests of stores mounted beneath wings or
fuselages are made, or when dynamic wind-tunnel tests to study the bomb
breakaway characteristics are made, the models used are usually limited
in size and, hence, operate at very low Reynolds numbers. The purpose
of these tests was to obtain the aerodynamic characteristics of store
or bomb configurations of three fineness ratios at Reynolds numbers
encountered in the bomb-drop investigations conducted in the Langley
9-inch supersonic tunnel and to determine the variation of the aerodynamic
characteristics with further increases in Reynolds number. These tests
were made at M = 1.62 and cover a Reynolds number range from 0.40×10^6
to 9.68×10^6, based on closed body length. Normal forces, chord forces,
and pitching moments were obtained for the bodies with fins of two dif-
ferent plan forms and without fins at angles of attack from -4° to 10°.
Schlieren photographs were taken to aid in the analysis of the data.

SYMBOLS

B configuration of body alone

BF configuration of body and fins

C chord force

C_C chord-force coefficient with base pressure converted to free-
               stream static pressure, Net chord force/qS

$(C_C)_o$ chord-force coefficient at $\alpha = 0^\circ$

C_m pitching-moment coefficient, (See fig. 1(a) for pitching-
               moment references), Pitching moment/qSl

$C_{m_\alpha} = \dfrac{\partial C_m}{\partial \alpha}$

$(C_{m_\alpha})_o$ C_{m_α} at $\alpha = 0^\circ$

C_N normal-force coefficient, Normal force/qS

$$C_N' = \frac{\text{Normal force}}{qS_F}$$

$$C_{N_\alpha} = \frac{\partial C_N}{\partial \alpha}$$

$$c_{N_\alpha}' = \frac{\partial C_N'}{\partial \alpha}$$

$\left(C_{N_\alpha}\right)_0$ C_{N_α} at $\alpha = 0^\circ$

d   maximum body diameter

l closed body length (8.110 in.)

l/d fineness ratio of closed body

M   free-stream Mach number

N   normal force

P   pitching moment

q   free-stream dynamic pressure

R   test Reynolds number, based on closed body length l

S   maximum body cross-sectional area

S_F exposed plan-form area of two fins

x   center-of-pressure position relative to nose of model, positive
                    rearward

α angle of attack

APPARATUS AND TESTS

Wind Tunnel

All tests were made in the Langley 9-inch supersonic tunnel. The tunnel is a continuous-operation, complete-return type in which the

pressure may be varied and controlled from about 1/10 atmosphere to
about 4 atmospheres stagnation pressure. Temperature and humidity condi-
tions may also be varied and controlled. The Mach number is varied by
interchanging nozzle blocks which form test sections approximately
9 inches square. A schlieren system is provided for qualitative visual-
flow observations.

Model Description

The dimensions and designations of the various models tested are
given in figure 1. Each of the bodies of models 1 and 2 consisted of
two tangential circular arcs of revolution so selected that the bodies
would have fineness ratios of 5 and 7, respectively, with the maximum
body diameters at 40 percent of the closed body length. Model 3 is a
0.045-scale model of the Douglas Aircraft Company store (see ref. 1)
with the maximum body diameter at 40 percent length. The fin plan form
of model 3 was also utilized in models 1 and 2 (see fig. 1(b)) and is
referred to as the "smaller" fin throughout this report. This fin plan
form was enlarged and modified somewhat for use with models 1A, 2A,
and 3A.

It was necessary to provide a cutoff at the rear of each body to
facilitate the sting mount which extended from the internal balances to
the model mount behind the body. The base diameters of all models were
0.157 inch. In general, the measured dimensions of the bodies and
fins were within ±0.005 inch of the specified dimensions given in fig-
ure 1 with the exception of the body radii which were found to be within
±0.001 inch.

The bodies of the three models were constructed of magnesium with
four slots 90° apart extending forward from the base in order that the
fins might be installed or removed. With the fins installed, the fin-
body juncture was faired with an epoxy resin adhesive. For the body-
alone tests, the slots were filled with the adhesive and faired to the
proper body contour.

Model and Balance Installation

Presented in figure 2 is a drawing of the model and balance installa-
tion. A selected model angle-of-attack reference point was adjusted lat-
erally at each test angle of attack so that this reference point would be
on the center line of the tunnel (see fig. 2). This was done in an effort
to utilize a longer model for a given tunnel width and Mach number with-
out the reflections of the disturbance from the model nose intersecting
the after portions of the model or fins. It was noted, however, that

the reflected shocks did intersect the tips of the tail fins of models 1
and 1A at the lowest Reynolds number of the tests. An optical angle-of-
attack system was used in conjunction with a 1/16-inch-diameter mirror
on the surface of each model; corrections were made for the effects of
the glass window upon the indicated angles of attack.

Three internal strain-gage balances were used in these investiga-
tions. One balance that measured a maximum of 2 pounds normal force
and 2 inch-pounds pitching moment was used to obtain those measurements
at the lowest test Reynolds number $\left(R = 0.40 \times 10^6\right)$ for all models tested
and at $R = 1.65 \times 10^6$ for tests of models 1, 2, and 3. For all other
measurements of normal force and pitching moment, a similar balance
with maximum design loads of 22 pounds normal force and 22 inch-pounds
pitching moment was used. A third balance capable of measuring 16 pounds
chord force was used to obtain the chord forces of all models at all the
test Reynolds numbers; simultaneously, the base pressure was measured so
that the base drag might be reduced to zero in the calculation of the
chord forces.

Tests

In order to obtain the complete normal-force, chord-force, and
pitching-moment characteristics of any one configuration throughout the
entire test Reynolds number range, it was necessary to interchange the
three internal strain-gage balances and make three separate test runs.

A part of the test program was devoted to obtaining the normal-
force and pitching-moment characteristics of models 1, 2, and 3 at
Reynolds numbers of 0.40×10^6 and 1.65×10^6 with boundary-layer transi-
tion artificially induced by using a transition ring installed about
1/4 inch behind the nose of the models. This ring consisted of fine
salt crystals sparsely distributed in a single layer about 1/8 inch wide
and about 1/64 inch thick.

Schlieren photographs were taken to aid in the analysis of the
measured data.

PRECISION OF DATA

All models were initially referenced with respect to the tunnel
walls within ±0.04°; angles of attack with respect to each other in a
given run were accurate to within ±0.01°. Surveys of the test section
of the $M = 1.62$ nozzle have shown that the maximum variation in Mach

number is ±0.01 and that the portion of the test section occupied by these models has maximum flow inclinations at any test pressure of between 0° and 0.25°. A summary of the estimated range of maximum probable errors is presented in the following table:

Models	Coefficients	Range of maximum probable errors		
		Balance 1 ($N = 2$ lb; $P = 2$ in-lb) $R = 0.4 \times 10^6$ to 1.6×10^6	Balance 2 ($N = 22$ lb; $P = 22$ in-lb) $R = 1.6 \times 10^6$ to 9.7×10^6	Balance 3 ($C = 16$ lb) $R = 0.4 \times 10^6$ to 9.7×10^6
1	C_N C_m C_C	0.0023 to 0.0006 0.00022 to 0.00005 ------------	0.0035 to 0.0005 0.00030 to 0.00005 ------------	------------ ------------ 0.0200 to 0.0007
2	C_N C_m C_C	0.0046 to 0.0011 0.00043 to 0.00010 ------------	0.0068 to 0.0011 0.00058 to 0.00009 ------------	------------ ------------ 0.0400 to 0.0015
3	C_N C_m C_C	0.0069 to 0.0016 0.00064 to 0.00015 ------------	0.0102 to 0.0016 0.00088 to 0.00014 ------------	------------ ------------ 0.0604 to 0.0022

RESULTS AND DISCUSSION

Presented in figures 3 to 11 are the measured aerodynamic characteristics of the configurations tested; in figure 12 are presented the center-of-pressure positions at angles of attack; in figure 13 are presented C_{N_α}, C_C, and center-of-pressure position at $\alpha = 0^\circ$ as a function of Reynolds number; in figures 14 and 15 are presented the incremental characteristics (BF - B) as a function of Reynolds number at $\alpha = 0^\circ$. Schlieren photographs taken at various Reynolds numbers are presented in figure 16; three sting lengths were used to support model 1. In table I is a summary of the measured aerodynamic characteristics at $\alpha = 0^\circ$.

In order to obtain more realistic center-of-pressure positions, especially at low angles of attack (see fig. 12), the curves of C_N and C_m were translated so that their increments at $\alpha = 0^\circ$ were removed.

These increments were primarily the result of inadvertent incidence in the fins.

Models 1, 2, and 3 Without Fins

Measured characteristics at angles of attack.- For the models without fins (see figs. 3 to 5) C_{N_α} was constant at each Reynolds number throughout the angle-of-attack range of from -2^O to 2^O. As the angle of attack increased beyond 2^O the effects of the viscous crossflow and the low-pressure recovery on the lee side of the afterbody resulted in a low-pressure increment on the afterbody (see ref. 2) and, consequently, an increase in C_{N_α} and C_C. Also, a rearward shift in the center-of-pressure position with increasing α was evident for the three body configurations at all Reynolds numbers with the exception of model 3 at $R = 1.65 \times 10^6$ (see fig. 12(a)).

These rearward center-of-pressure shifts, due to the angle-of-attack effects, began at relatively low angles of attack for the $R = 0.40 \times 10^6$ tests; then, as R increased to $R = 1.65 \times 10^6$, the rearward center-of-pressure shift did not occur until a higher angle of attack was reached. This was due to the reduction of the laminar separation at the higher Reynolds number as indicated in figs. 16(a), 16(b), and 16(c). Further increases in Reynolds number resulted in the rearward center-of-pressure shift occurring at lower angles of attack, probably due to the formation of the turbulent boundary layer accompanied by a pair of symmetrically disposed vortices forming on the lee side of the afterbody (see ref. 2) and contributing to the negative-pressure increment associated with the viscous crossflow effects.

Measured characteristics at $\alpha = 0^O$.- The variation of C_{N_α}, C_C, and center-of-pressure position with Reynolds number at $\alpha = 0^O$ are presented in figure 13(a). A reduction in C_{N_α} and a forward movement in the center-of-pressure position with an increase in Reynolds number up to $R = 2.95 \times 10^6$ for model 1 and $R = 5.55 \times 10^6$ for models 2 and 3 is indicated. These large variations are the result of the flow remaining attached to the surface of the afterbodies longer as R increases (see fig. 16(a)), thereby reducing the lifting pressure increments usually associated with separated flow over the afterbody; this, of course, is accompanied by a forward movement of the center-of-pressure position. The schlieren photographs in figure 16 indicate that boundary-layer transition over the rearward portion of the afterbody occurs at the Reynolds numbers where the variation in C_{N_α} and center-of-pressure position with R becomes small. Further increases in R have little effect upon these characteristics.

A large variation in C_C at $\alpha = 0^\circ$ was indicated for all three bodies as R increased from 0.40×10^6 to 1.65×10^6; within this Reynolds number range, the station of flow detachment moved rearward rapidly as R increased (see fig. 16(a)) and more of the afterbody became subjected to the negative pressures realized as the flow expanded around the body contour. Consequently, C_C increased rapidly due to this increase in pressure drag. Further increases in R above $R = 1.65 \times 10^6$ resulted in minor increases in C_C due primarily to changes in skin friction.

Models 1, 2, and 3

Measured characteristics at angles of attack.- In figures 6 to 8 it is shown that, for configurations tested, C_N and C_m were linear in the angle-of-attack range of from -1° to 1°. As would be expected, the rate at which C_{N_α} increased with α beyond 1° was dependent upon a combination of the body-alone characteristics and the blanketing effects of the body upon the fins. At all test Reynolds numbers where the results are available, C_N was again linear with α at angles of attack greater than 6°. In a manner similar to the results of the tests of the bodies without fins, C_C increased with α and the substitution of the larger fins for the smaller ones, in general, resulted in a decrease in the rate with which C_C increased with α.

The variations of the center-of-pressure positions of models 1, 2, and 3 with α (see fig. 12(b)) were also dependent upon the characteristics of the models without fins and the blanketing effects of the body upon the fins. The rearward center-of-pressure movement due to α was delayed to $\alpha = 5^\circ$ at $R = 0.40 \times 10^6$ for model 1 because of the large region of separated flow within which the fins operated (see fig. 16(d)). For models 2 and 3, the separated flow blanketed smaller portions of the fins, and the rearward center-of-pressure movement took place at lower angles of attack ($\alpha \approx 2^\circ$). Increases in the test Reynolds number beyond $R = 0.40 \times 10^6$ reduced the region of low dynamic pressure within which a portion of the fins operated and resulted in either an earlier rearward center-of-pressure movement or no movement at all. Comparisons of these results (see fig. 12(b)) also indicated that the center-of-pressure positions for an individual model at various Reynolds numbers tended to converge at angles of attack of about 10°, 8°, and 7° corresponding to values of x/l of about 0.40, 0.53, and 0.60 for models 1, 2, and 3, respectively. Further increases in α had negligible effects upon the center-of-pressure position.

Measured characteristics at $\alpha = 0^\circ$.- Shown in figure 13(b) are the results of tests of models 1, 2, and 3 at $\alpha = 0^\circ$. In the case of model 1, the addition of the fins was just sufficient to overcome the reduction in C_{N_α} noted in figure 13(a) for model 1 without fins between $R = 0.40 \times 10^6$ and $R = 2.95 \times 10^6$. This means that the loss of normal force realized by the body alone due to the flow remaining attached longer at the higher Reynolds numbers was exactly supplemented by the additional normal force gained by the increase in fin area outside of the separated flow region. Consequently, the incremental normal-force coefficient, $\left(C_{N_\alpha}\right)_{BF-B}$ increased with Reynolds number within this Reynolds number range (see fig. 14(a)). The forward center-of-pressure movement of model 1 without fins was greatly reduced by the addition of the fins due to their increase in effectiveness as R increased to a value of 2.95×10^6. Further increase of the Reynolds number to $R = 9.70 \times 10^6$ had no effect on C_{N_α} for model 1 although the center-of-pressure position moved forward from $x/l = 0.29$ to $x/l = 0.23$ resulting in a negative increment of $(x/l)_{BF-B}$ (fig. 14(a)) within this Reynolds number range.

In the case of models 2 and 3, which had much thinner boundary layers in the regions occupied by the fins as compared with model 1, the addition of the fins more than compensated for the reduction of C_{N_α} of body-alone up to $R = 5.55 \times 10^6$ and, therefore, C_{N_α} increased and the center-of-pressure position moved rearward. Further increases in R resulted in small reductions in C_{N_α} and slight forward shifts in the center-of-pressure position; consequently, the incremental aerodynamic characteristics of models 2 and 3 in figure 14(a) showed substantial increases in $\left(C_{N_\alpha}\right)_{BF-B}$ and large positive increments in $(x/l)_{BF-B}$ from $R = 0.40 \times 10^6$ to $R = 5.55 \times 10^6$, and minor variations with further increase in R.

The variations of C_C with Reynolds number for models 1, 2, and 3 were similar to the C_C variations of the bodies alone (compare figs. 13(a) and 13(b)). Because the incremental chord-force coefficients are of such low magnitudes, no analyses of these results are attempted but remain to be discussed in general along with the discussion of $\left(C_C\right)_{BF-B}$ for models 1A, 2A, and 3A.

Models 1, 2, and 3 With Artificial Transition

The purpose of these tests was to determine how the results of low Reynolds number tests of these configurations with transition induced artificially would compare with the results of high Reynolds number tests of the same configurations with natural transition. Direct comparisons of the results obtained are presented in figure 13(b). Also, a summation of these comparative results is presented in the table to follow. The percentage difference in $\left(C_{N_\alpha}\right)_0$ represents the $\left(C_{N_\alpha}\right)_0$ measured at the low Reynolds number with artificial transition minus the $\left(C_{N_\alpha}\right)_0$ measured at $R = 9.70 \times 10^6$ with natural transition as a percentage of the latter; the difference in x/l represents the difference in the center-of-pressure positions between that measured at the low Reynolds number with artificial transition and that measured at $R = 9.70 \times 10^6$.

Model	Reynolds number	Difference in $\left(C_{N_\alpha}\right)_0$, percent	Difference in x/l
1	0.40×10^6	0	0.15
2	.40	-11	-.03
3	.40	-14	-.07
1	1.65×10^6	-21	-.09
2	1.65	-11	.01
3	1.65	-3	-.01

It is shown that for the tests at $R = 0.40 \times 10^6$ the percentage difference in $\left(C_{N_\alpha}\right)_0$ as well as the difference in x/l increases negatively as the fineness ratio increases. The opposite was apparent for the results of the tests at $R = 1.65 \times 10^6$. Of this group of comparative results, only the results of model 3 at $R = 1.65 \times 10^6$ fall within desirable accuracies for both $\left(C_{N_\alpha}\right)_0$ and x/l. Therefore, it may be concluded that these comparisons indicated no justification for testing such configurations with a transition ring installed at these low Reynolds numbers and for expecting duplication of the results obtained at high Reynolds numbers with natural transition. Schlieren observations for model 1 indicated that at a Reynolds number of 0.40×10^6 the transition ring did not cause transition or significantly alter the degree of separation.

Models 1A, 2A, and 3A

Measured characteristics at angles of attack.- The results of tests
of models 1A, 2A, and 3A indicated that the effects of variations in
angle of attack upon the measured aerodynamic characteristics were similar
to those of models 1, 2, and 3 except that the blanketing effects of the
bodies upon the fins were not as severe for these models having the larger-
span fins (for instance, compare fig. 12(b) with 12(c)). The center-of-
pressure positions for models 1A, 2A, and 3A (with the larger fins) at
various Reynolds numbers tended to converge at angles of attack of 9°,
5°, and 3° at values of x/l of 0.57, 0.66, and 0.73, respectively, (see
fig. 12(c)). These angles of attack were lower than those indicated for
the models with the smaller fins, particularly in the cases of those
utilizing the higher-fineness-ratio bodies.

Measured characteristics at $\alpha = 0^o$.- Presented in figure 13(c) are
the measured characteristics at $\alpha = 0^o$ for models 1A, 2A, and 3A. For
all three models, the addition of the larger fins more than compensated
for the loss in $\left(C_{N_\alpha}\right)_o$ with increases in Reynolds number of the body
alone; and $\left(C_{N_\alpha}\right)_o$ increased as the Reynolds number increased up to
about 3×10^6 beyond which the curves were essentially flat. These gains
were due to the over-all increase in effectiveness of the fins as R
increased in the low Reynolds number range; consequently, $\left(C_{N_\alpha}\right)_{BF-B}$
increased with Reynolds number throughout the low Reynolds number range
(see fig. 14(b)) with little or no increase in the medium and high
Reynolds number ranges.

The forward center-of-pressure movement of model 1 without fins was
completely overcome, and the center-of-pressure position of model 1A was
stationary throughout the entire test Reynolds number range; also, the
center-of-pressure movements of models 2A and 3A were rearward up to
Reynolds numbers of about 3×10^6, with no significant effects due to
further increases in Reynolds numbers. In conjunction with the charac-
teristics of $\left(C_{N_\alpha}\right)_{BF-B}$ for these configurations, the variations in
$(x/l)_{BF-B}$ with increasing Reynolds number (see fig. 14(b)) were positive
up to $R = 2.95 \times 10^6$ for model 1A and up to $R = 5.55 \times 10^6$ for
models 2A and 3A with no effects due to further increases in Reynolds
number.

The C_C results presented in figure 13(c) again indicate the
characteristic sharp rise in C_C with increasing R in the low R range.
Comparison of figures 13(b) and 13(c) suggests that the mutual chord-
force interferences of body and fins of models 2 and 3 are of appreciable
magnitude throughout most of the test R range. This is evidenced by
the fact that changing from the smaller to the larger fins not only

increased C_C but also changed the relative magnitudes of C_C with
varying Reynolds number. Evidence of the magnitude of the chord-force
interferences of models 1 and 1A at Reynolds numbers less than about
1.6×10^6 is indicated in figures 14(a) and 14(b). Although the region
of separated flows about the afterbody became smaller and exposed more
of the fins to the high-dynamic-pressure stream, $(C_C)_{BF-B}$ decreased
appreciably. This indicated that a decrease in chord force due to mutual
interference was evident and that this decrease was more than sufficient
to compensate for the increase in the chord force of the fins as R
increased from 0.4×10^6 to about 1.6×10^6. Such was not evident for
models 2, 2A, 3, and 3A.

Comparative Effectiveness of Small and Large Fins

Presented in figure 15 are the incremental normal-force coefficients
at $\alpha = 0^\circ$ based upon the exposed areas of two fin panels. These coef-
ficients are, therefore, a measure of the effectiveness of a particular
set of cruciform fins in the presence of a particular body for which one
set of fins lies in the plane of the angle of attack.

As expected, these results indicated that higher fin effectiveness
was obtained whenever larger portions of the lifting fin panels were
outside of the region of low-dynamic-pressure flow. This was evident
regardless of whether the fin effectiveness was increased by decreasing
the maximum diameter of the body, by increasing the Reynolds number
throughout the low Reynolds number range, or by enlarging the fins
(effectiveness of the large fins was about 1.8 times that of the small
ones throughout the test Reynolds number range). Also, the variations
in fin effectiveness due to changes in body shapes were much less for
the larger fins than for the small ones.

CONCLUSIONS

The results of tests at a Mach number of 1.62 of three bomb, or store,
shapes with and without two sets of cruciform fins indicated the following
conclusions:

(1) For those configurations without fins for which results were
obtained, the effects of increasing the angle of attack α outside the
low angle-of-attack range were to increase the change in normal-force
coefficient with angle of attack C_{N_α} and the chord-force coefficient C_C
above those values obtained at $\alpha = 0^\circ$ and to shift the center-of-pressure
position rearward; the angle of attack at which these variations took
place was dependent upon Reynolds number.

(2) For those configurations without fins, at $\alpha = 0^\circ$, the effects of increasing the test Reynolds number were to reduce significantly C_{N_α}, to increase C_C, and to shift the center-of-pressure position forward until the Reynolds number for transition was reached, beyond which small variations in C_{N_α} and center-of-pressure position were evident.

(3) For the finned configurations the effects of angle of attack at the majority of the test Reynolds numbers were to increase C_{N_α} and C_C above those values at $\alpha = 0^\circ$ and to shift the center-of-pressure position rearward until some intermediate angle of attack was reached; at this angle, and at higher angles of attack, the center-of-pressure positions at all Reynolds numbers were about the same for each finned configuration.

(4) The effects of increasing Reynolds number upon the majority of the finned configurations at $\alpha = 0^\circ$ were to increase C_{N_α} until the Reynolds number for transition was reached; at higher Reynolds numbers C_{N_α} at $\alpha = 0^\circ$ was about constant.

(5) The effects of increasing Reynolds number upon the center-of-pressure position of the finned configurations were decreased by utilizing the large fins.

(6) The fineness-ratio-8.6 model with small fins and all models with large fins were statically stable at all angles of attack and at all test Reynolds numbers about a typical center-of-gravity location assumed to lie at 45 percent of the closed body length.

(7) The results of these tests indicate that it is possible to design a supersonic bomb configuration having a constant C_{N_α} or center-of-pressure position or both for angles of attack near 0° and for Reynolds numbers of the order of 3×10^6 and greater.

Langley Aeronautical Laboratory,
    National Advisory Committee for Aeronautics,
        Langley Field, Va.

REFERENCES

1. Muse, T. C., and Bratt, R. W.: Summary of High Speed Wind-Tunnel
     Tests of a Douglas Aircraft Store Shape and a 2,000-Pound
     G.P.-AN-M66 Bomb. Rep. No. E.S. 21150, Douglas Aircraft Co., Inc.,
     June 25, 1948.

2. Allen, H. Julian, and Perkins, Edward W.: Characteristics of Flow
     Over Inclinded Bodies of Revolution. NACA RM A50L07, 1951.

TABLE I.- SUMMARY OF MEASURED AERODYNAMIC CHARACTERISTICS AT $\alpha = 0°$

Model	Reynolds number	c_{N_α}	c_C	Center-of-pressure position
1 (No fins)	0.40×10^6	0.0341	0.250	0.19
	1.65	.0333	.340	.10
	2.95	.0294	.343	0
	5.55	.0315	.351	.03
	7.65	.0310	.352	.04
	9.70	.0311	-----	.05
2 (No fins)	0.40	.0340	.116	.14
	1.65	.0342	.185	.09
	2.95	.0300	.187	0
	5.55	.0260	.206	-.15
	7.65	.0252	.222	-.16
	9.70	.0240	.229	-.17
3 (No fins)	0.40	.0350	.084	.07
	1.65	.0320	.160	-.02
	2.95	.0300	.173	-.11
	5.55	.0245	.190	-.32
	7.65	.0230	.218	-.31
	9.70	.0232	.220	-.33
1	0.40	.0428	.275	.34
	1.65	.0445	.351	.29
	2.95	.0447	.360	.29
	5.55	.0448	.364	.28
	9.70	.0433	.372	.23
2	0.40	.0521	.130	.40
	1.65	.0658	.195	.46
	2.95	.0617	.225	.43
	5.55	.0693	.233	.49
	9.70	.0642	.265	.46
3	0.40	.0744	.055	.49
	1.65	.0850	.177	.52
	2.95	.0870	.185	.55
	5.55	.0986	.227	.61
	9.70	.0959	.283	.59
1 (With transition)	0.40	.0435	.295	.33
	1.65	.0340	.370	.14
2 (With transition)	0.40	.0574	.149	.43
	1.65	.0570	.285	.47
3 (With transition)	0.40	.0822	.110	.50
	1.65	.0928	.306	.56
1A	0.40	.0630	.320	.52
	1.65	.0613	.353	.48
	2.95	.0727	.362	.53
	5.55	.0727	.380	.51
	7.65	.0697	.387	.50
	9.70	.0720	-----	.51
2A	0.40	.0915	.108	.61
	1.65	.1027	.259	.60
	2.95	.1075	.268	.63
	5.55	.1145	.282	.67
	7.65	.1145	.311	.66
	9.70	.1163	.320	.66
3A	0.40	.1430	.182	.68
	1.65	.1765	.269	.72
	2.95	.1805	.285	.71
	5.55	.1800	.341	.72
	7.65	.1790	.355	.71
	9.70	.1730	.360	.72
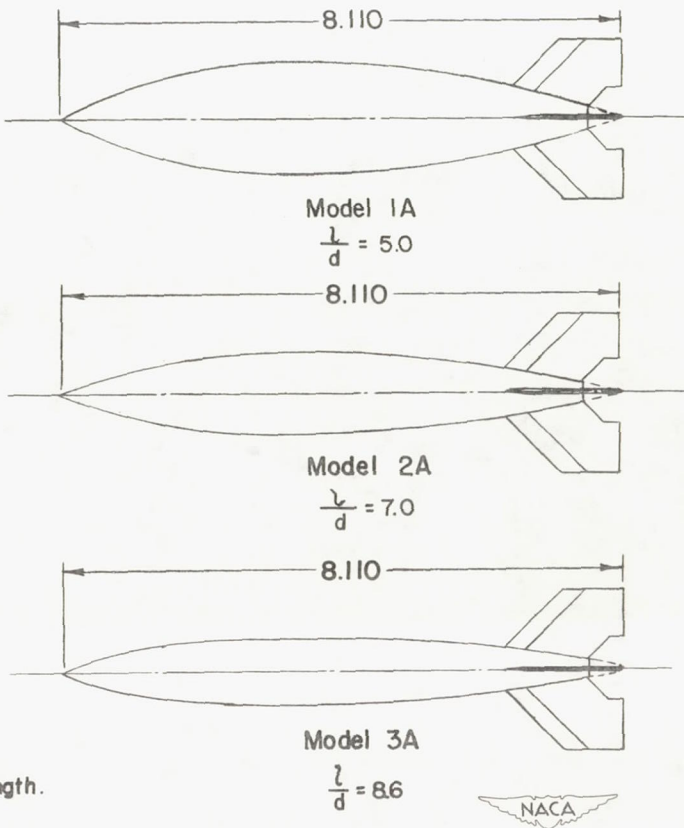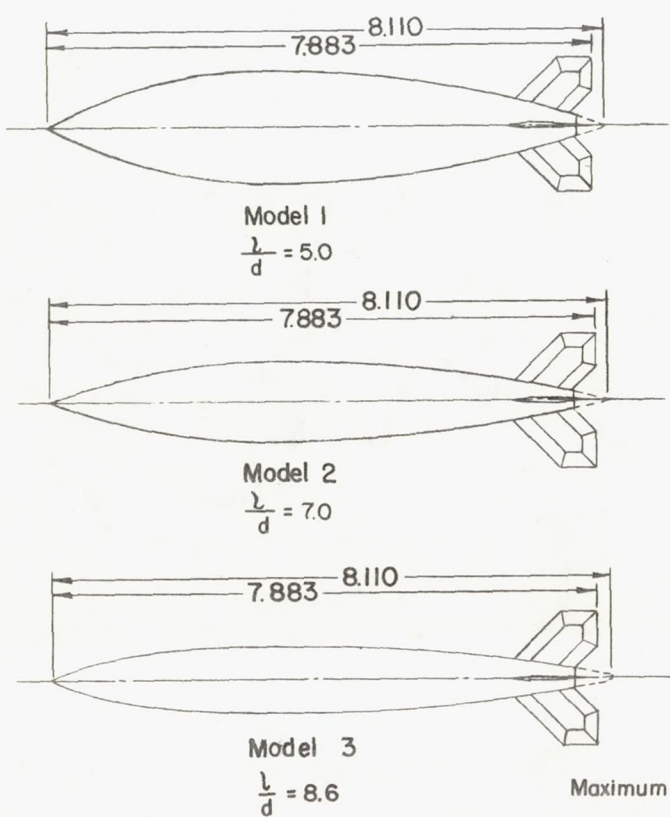
NACA

(a) Complete bomb configurations.

Figure 1.- Dimensions and designations of models.

.700

13.8°   13.8°

.057

Section A-A

.496

.969

A .473

45°   .992   45°

For Models 1, 2, and 3

.925

13.8°

.057

Section B-B

B

.863

1.146

B   .473

45°   1.309   45°   .227
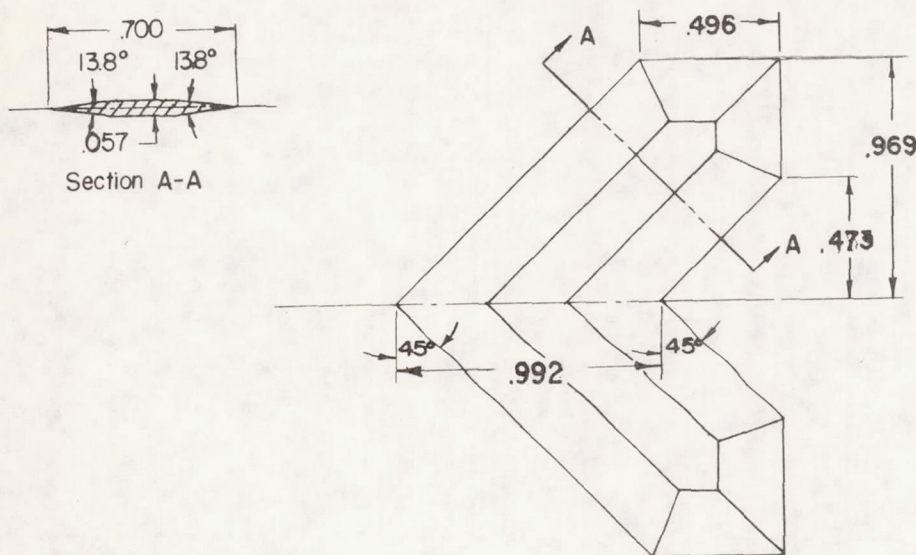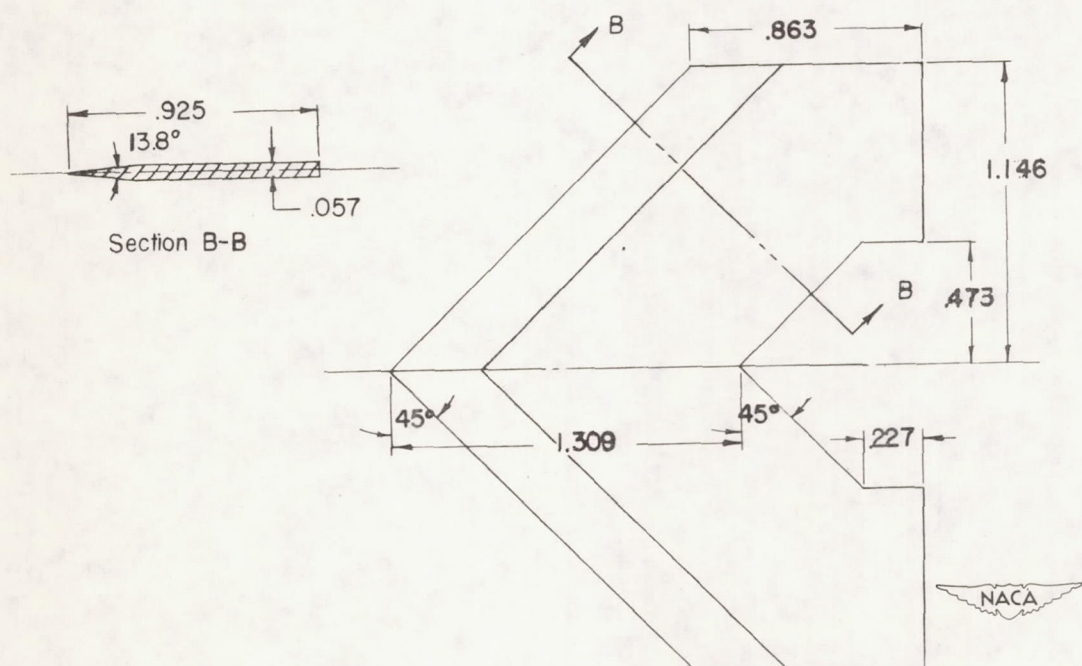
For Models 1A, 2A, and 3A

NACA

(b) Fin plan forms.

Figure 1.- Concluded.
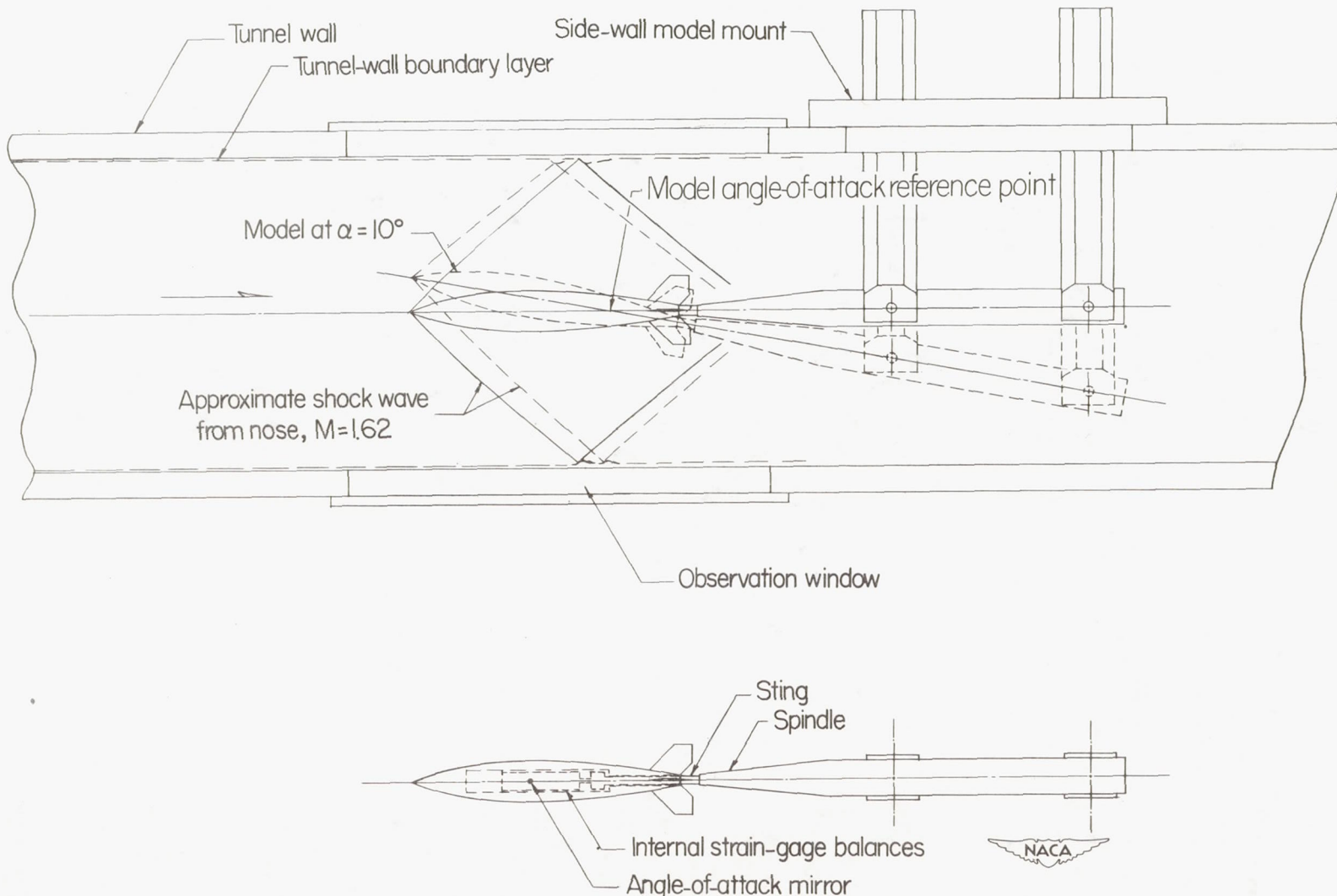
Figure 2.- Model and balance installation in the Langley 9-inch supersonic tunnel.
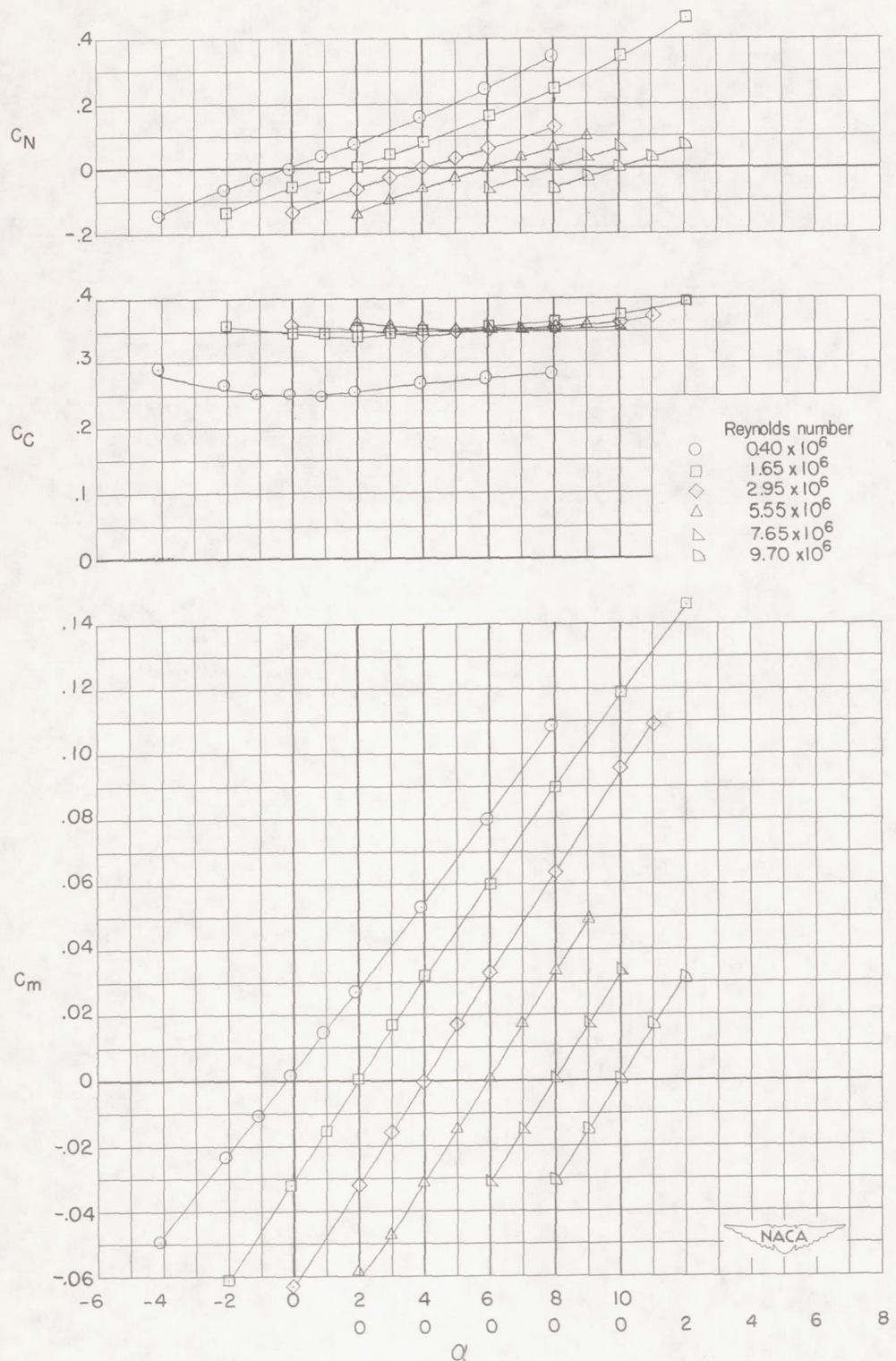
Figure 3.- Normal-force, chord-force, and pitching-moment characteristics of model 1 without fins at M = 1.62 and at various Reynolds numbers.
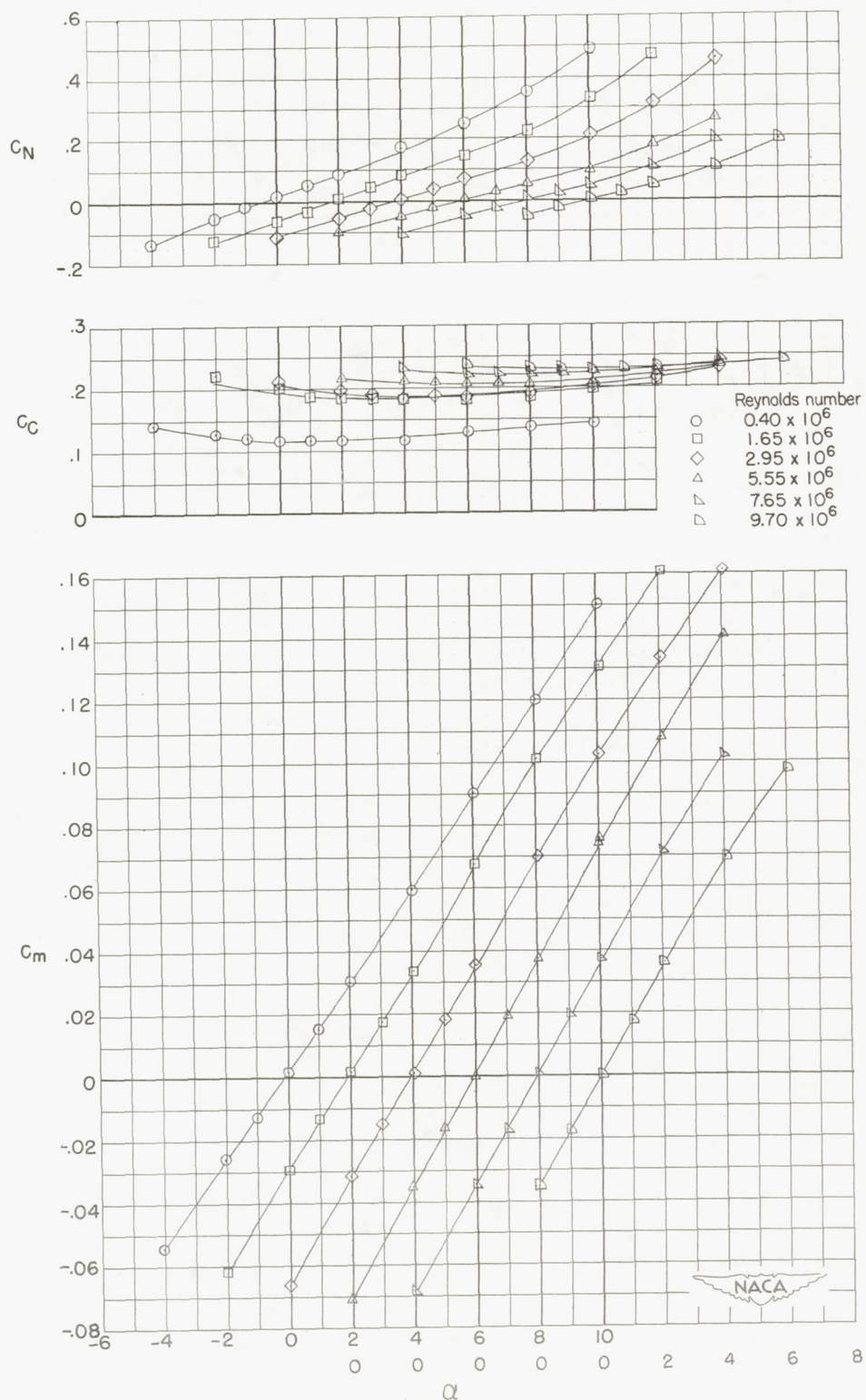
Figure 4.- Normal-force, chord-force, and pitching-moment characteristics
of model 2 without fins at M = 1.62 and at various Reynolds numbers.
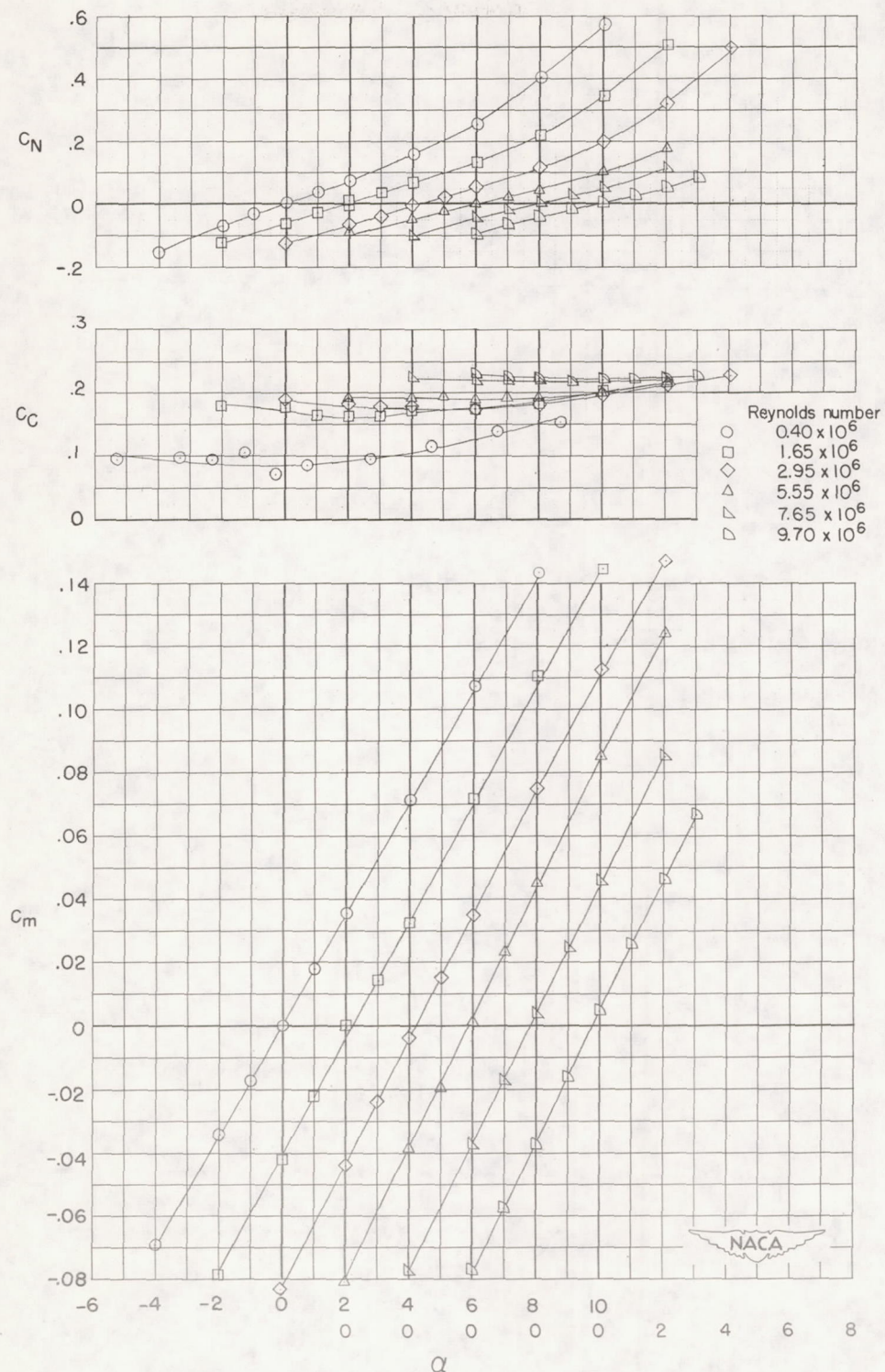
Figure 5.- Normal-force, chord-force, and pitching-moment characteristics of model 3 without fins at M = 1.62 and at various Reynolds numbers.
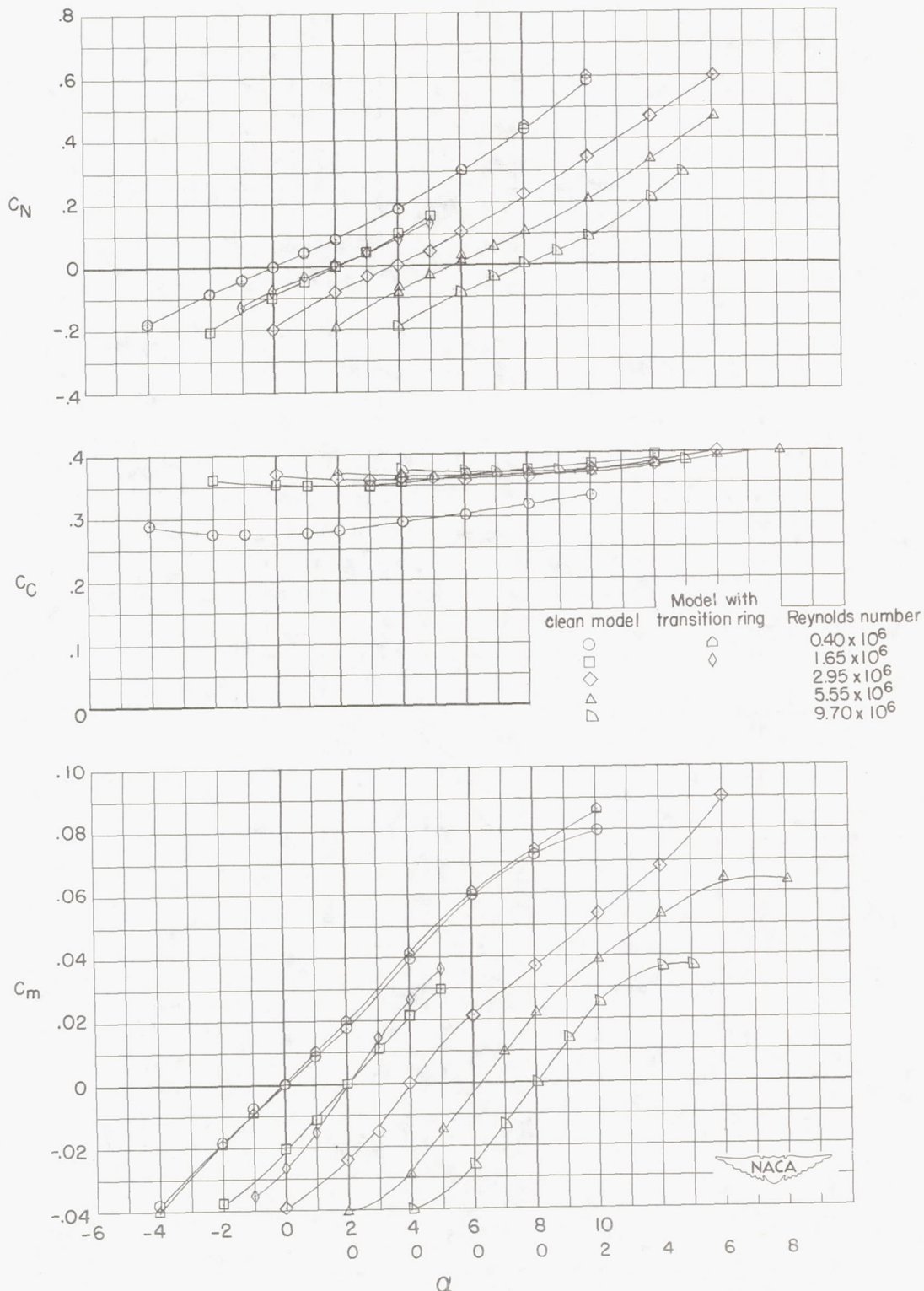
Figure 6.- Normal-force, chord-force, and pitching-moment characteristics
of model 1 at M = 1.62 and at various Reynolds numbers.
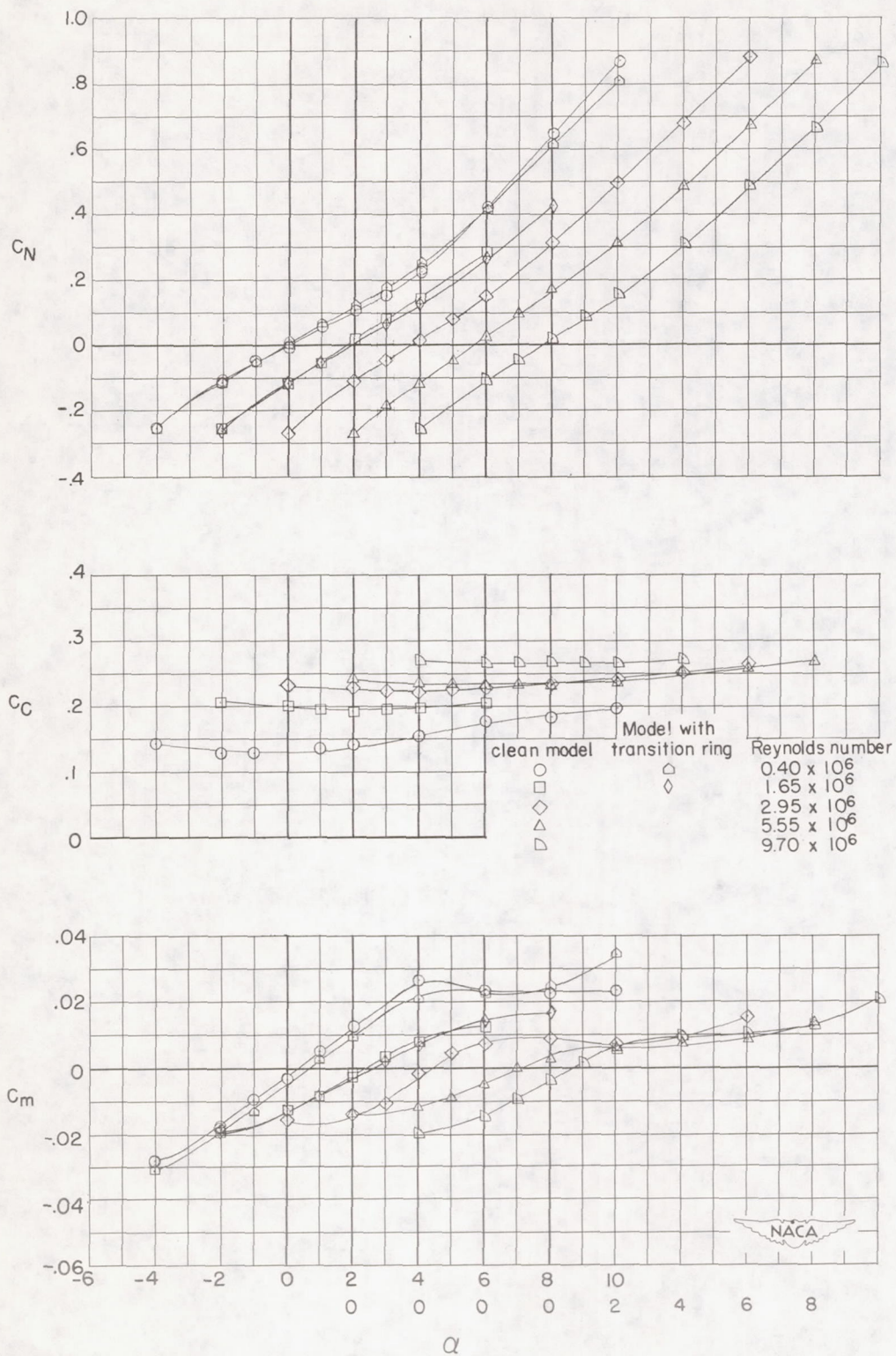
Figure 7.- Normal-force, chord-force, and pitching-moment characteristics
of model 2 at M = 1.62 and at various Reynolds numbers.
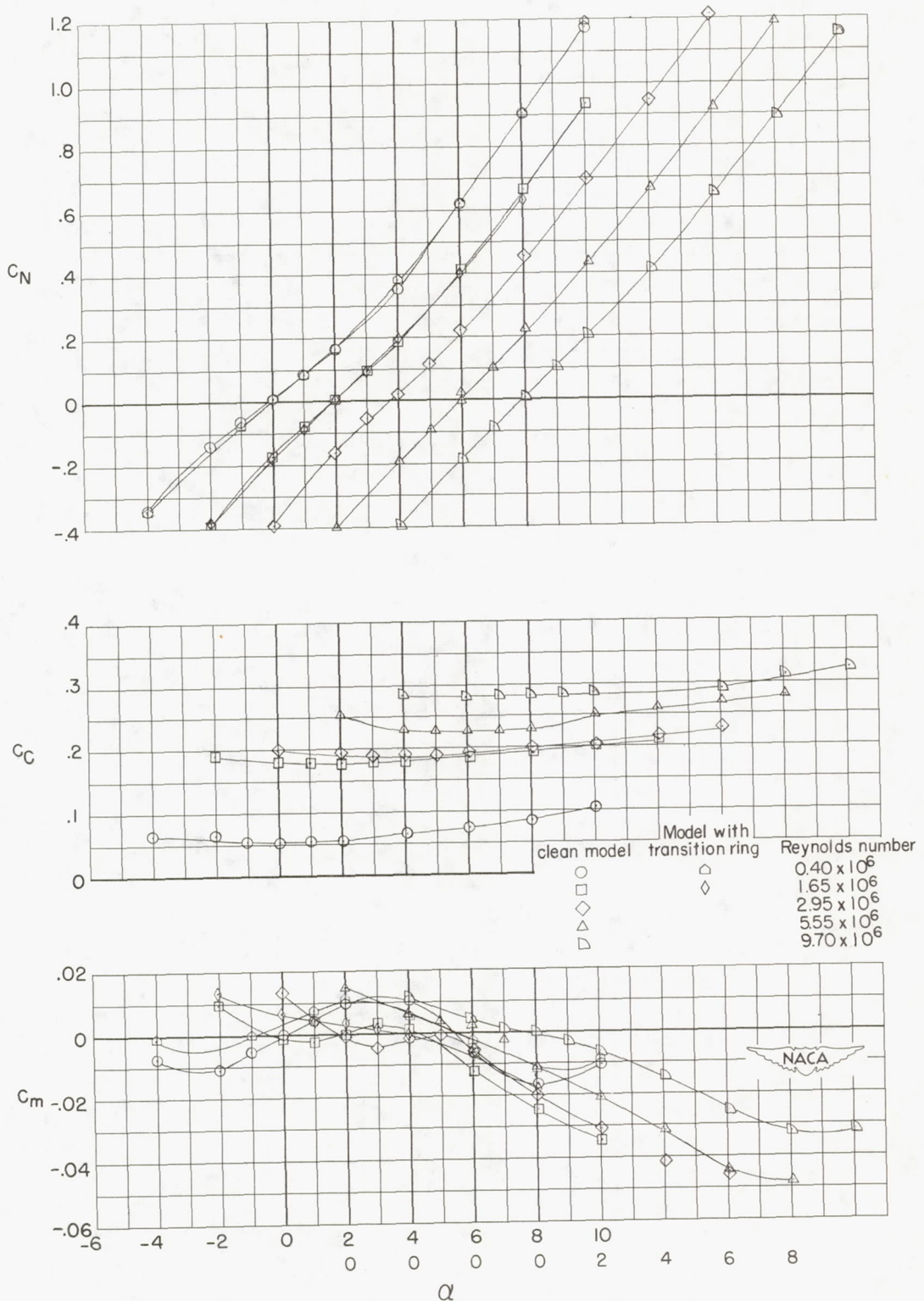
Figure 8.- Normal-force, chord-force, and pitching-moment characteristics of model 3 at M = 1.62 and at various Reynolds numbers.
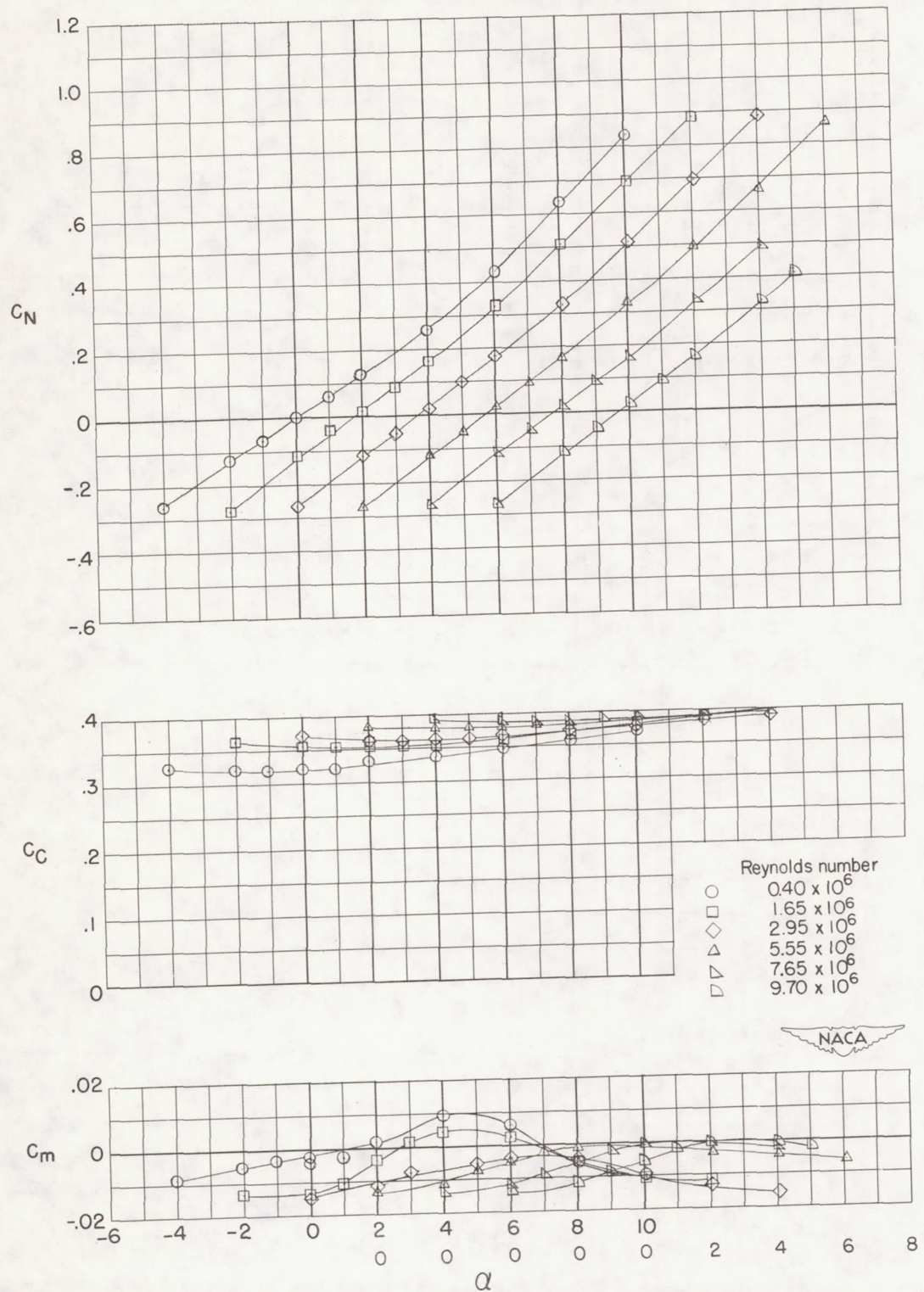
Figure 9.- Normal-force, chord-force, and pitching-moment characteristics
of model 1A at M = 1.62 and at various Reynolds numbers.
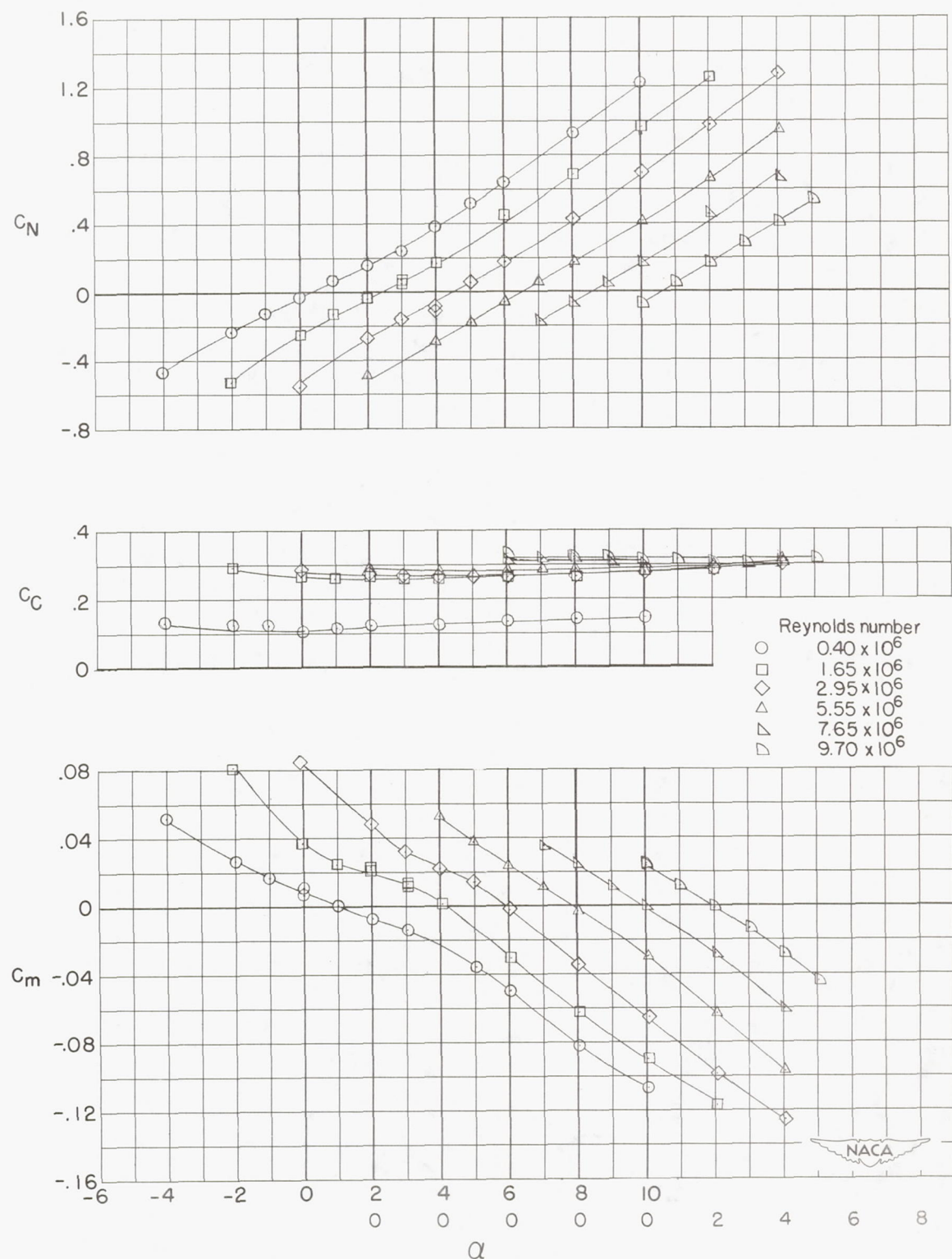
Figure 10.- Normal-force, chord-force, and pitching-moment characteristics
of model 2A at M = 1.62 and at various Reynolds numbers.
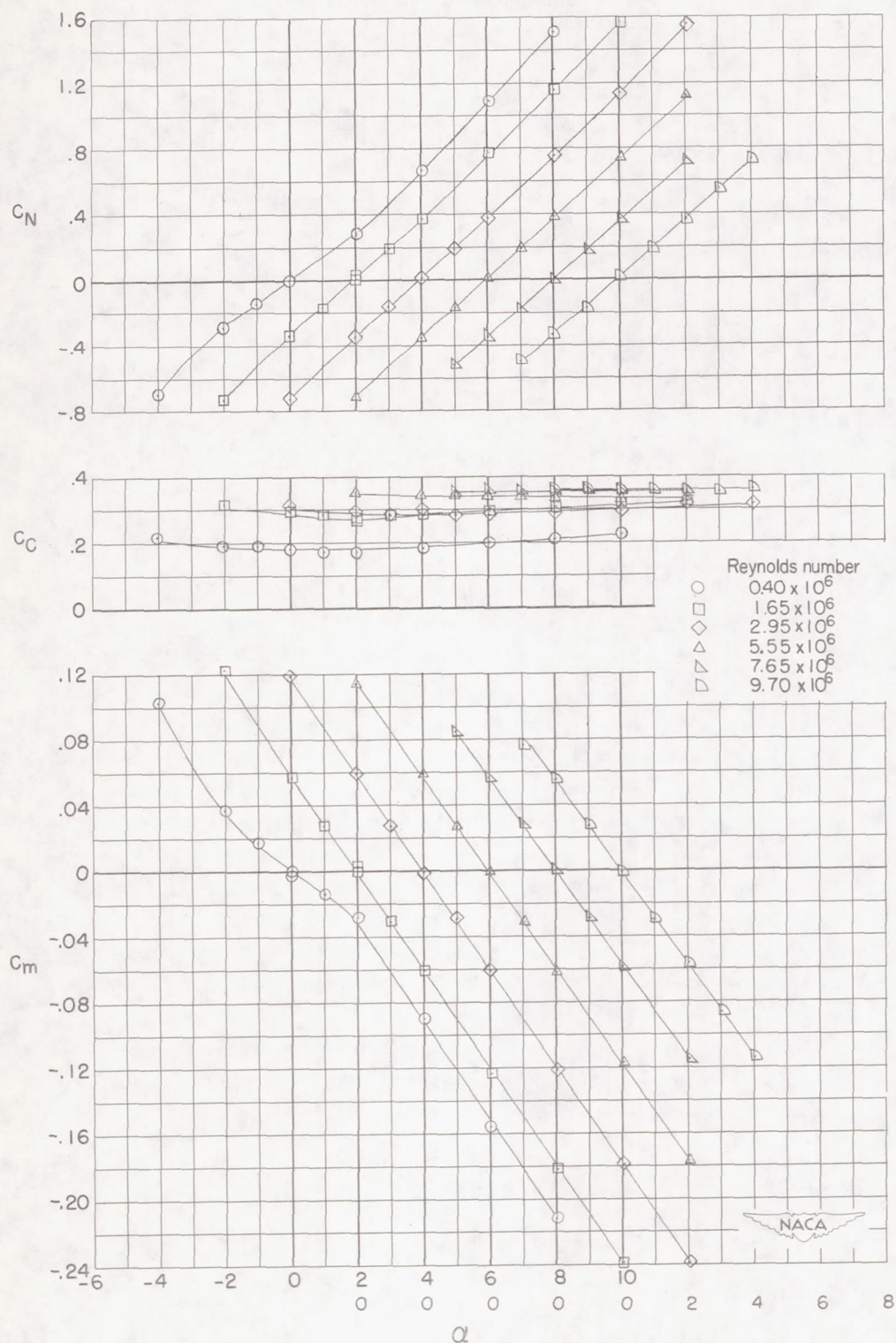
Figure 11.- Normal-force, chord-force, and pitching-moment characteristics
of model 3A at M = 1.62 and at various Reynolds numbers.
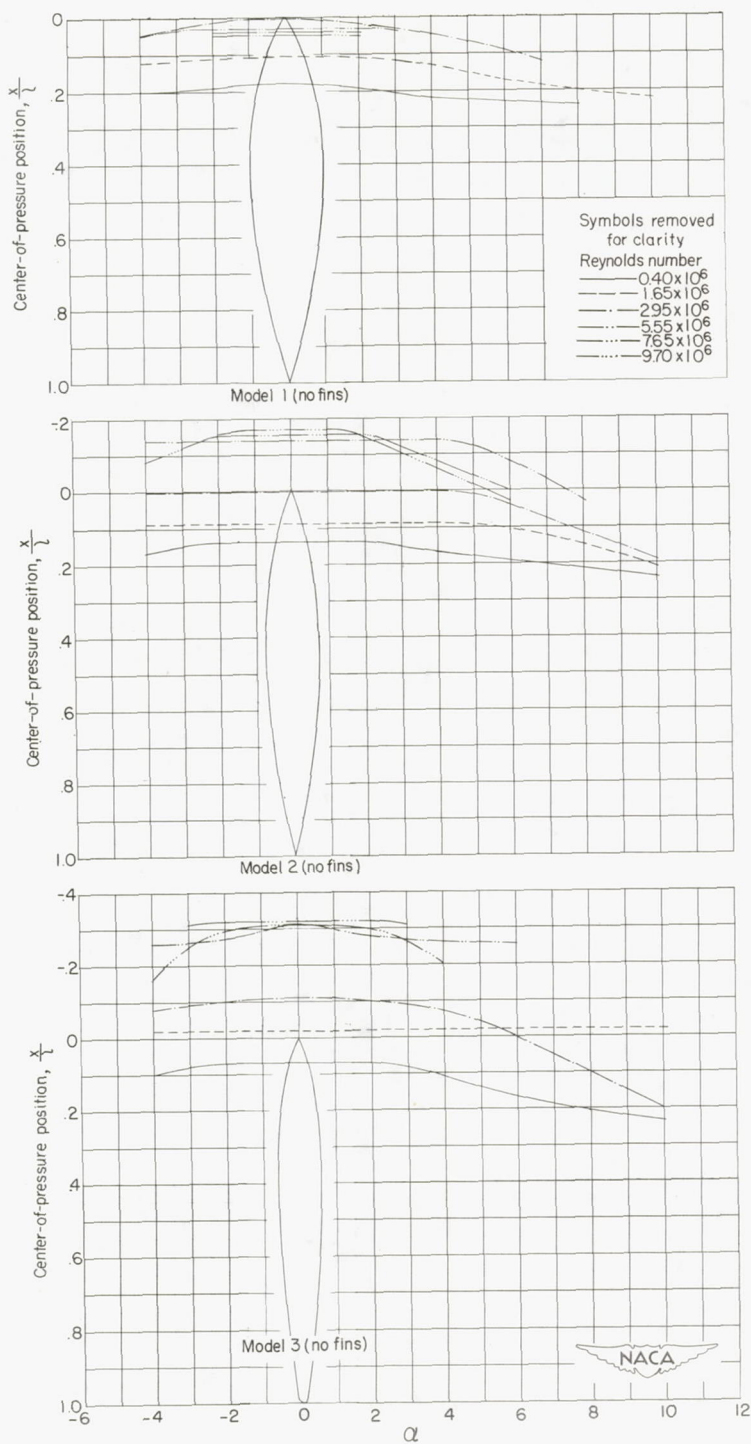
(a) Models 1, 2, and 3 (no fins).

Figure 12.- Center-of-pressure position of bomb or store models at various Reynolds numbers.

Symbols removed
for clarity

Reynolds number
——— 0.40 x 10⁶
— — 1.65 x 10⁶
—··— 2.95 x 10⁶
—···— 5.55 x 10⁶
—····— 9.70 x 10⁶

Model 1

Model 2

Typical center-of-gravity location

Model 3

NACA
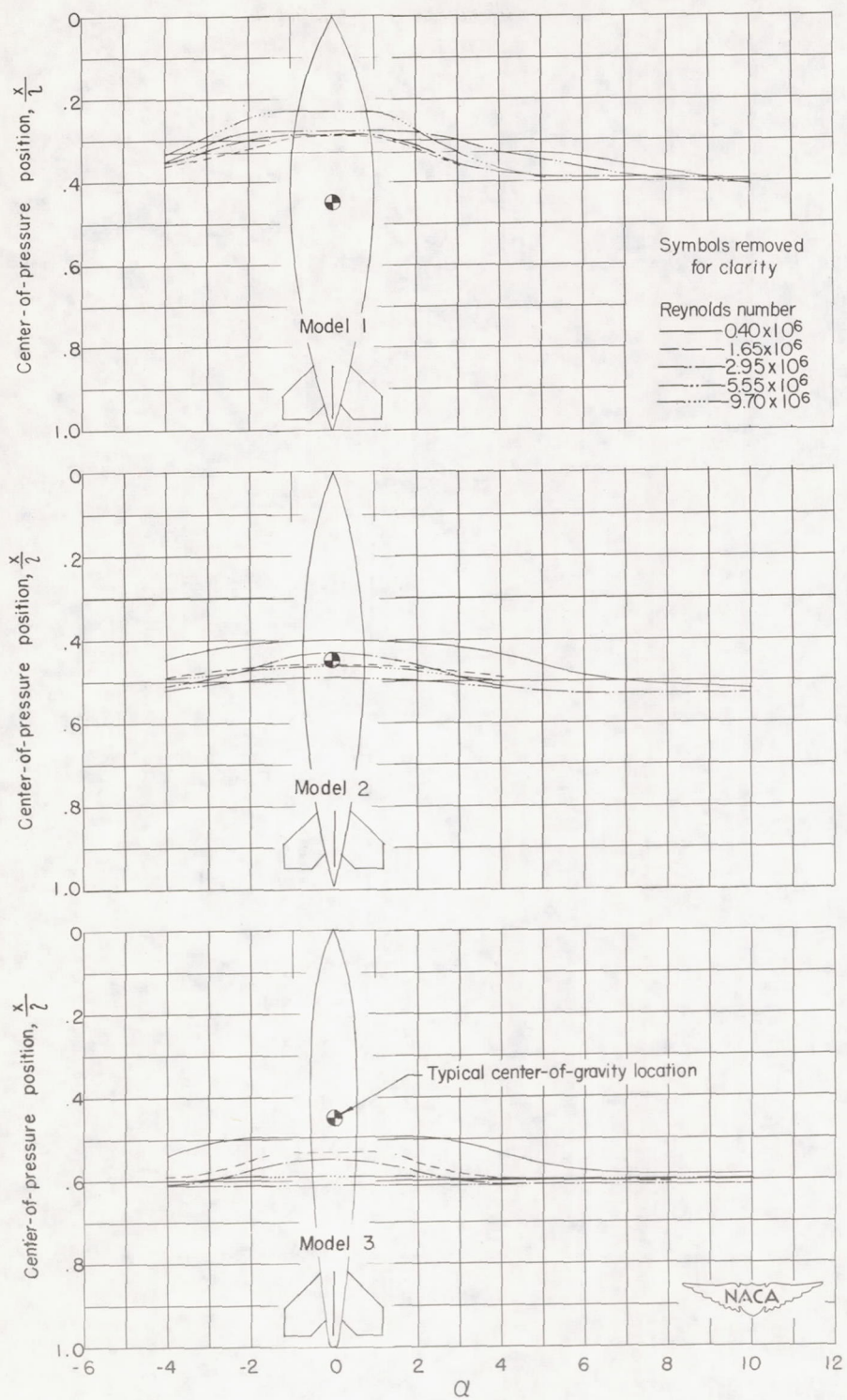
(b) Models 1, 2, and 3.

Figure 12.- Continued.
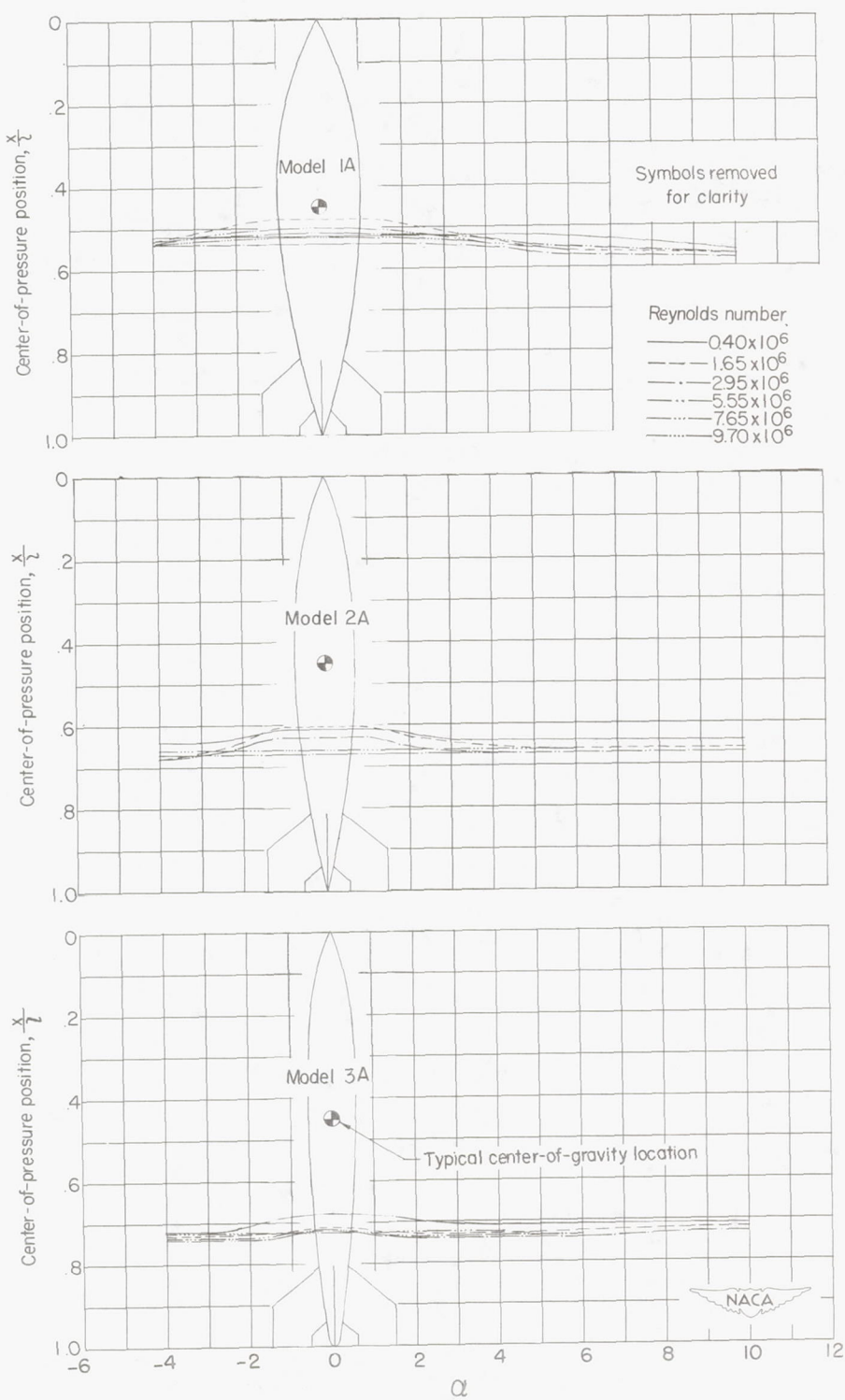
(c) Models 1A, 2A, and 3A.

Figure 12.- Concluded.
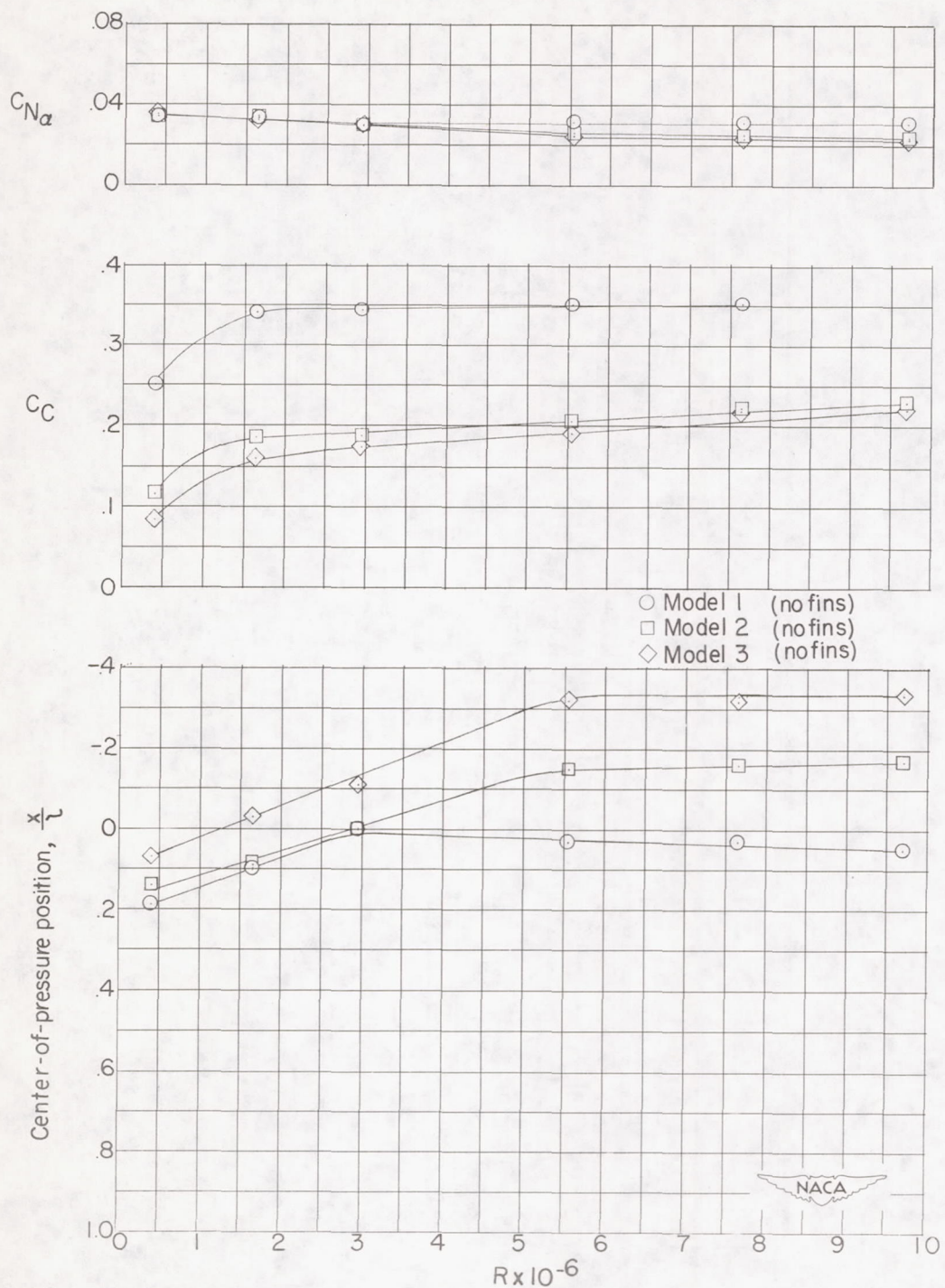
(a) Models 1, 2, and 3 (no fins).

Figure 13.- Variations of aerodynamic characteristics at $\alpha = 0°$ with
Reynolds number.

Clean   With transition ring
             △ Model 1, R = 0.40 x 10⁶
O Model 1   ⊿ Model 1, R = 1.65 x 10⁶
□ Model 2   ◣ Model 2, R = 0.40 x 10⁶
◇ Model 3   ◪ Model 2, R = 1.65 x 10⁶
             ◪ Model 3, R = 0.40 x 10⁶
             ◪ Model 3, R = 1.65 x 10⁶

R x 10⁻⁶
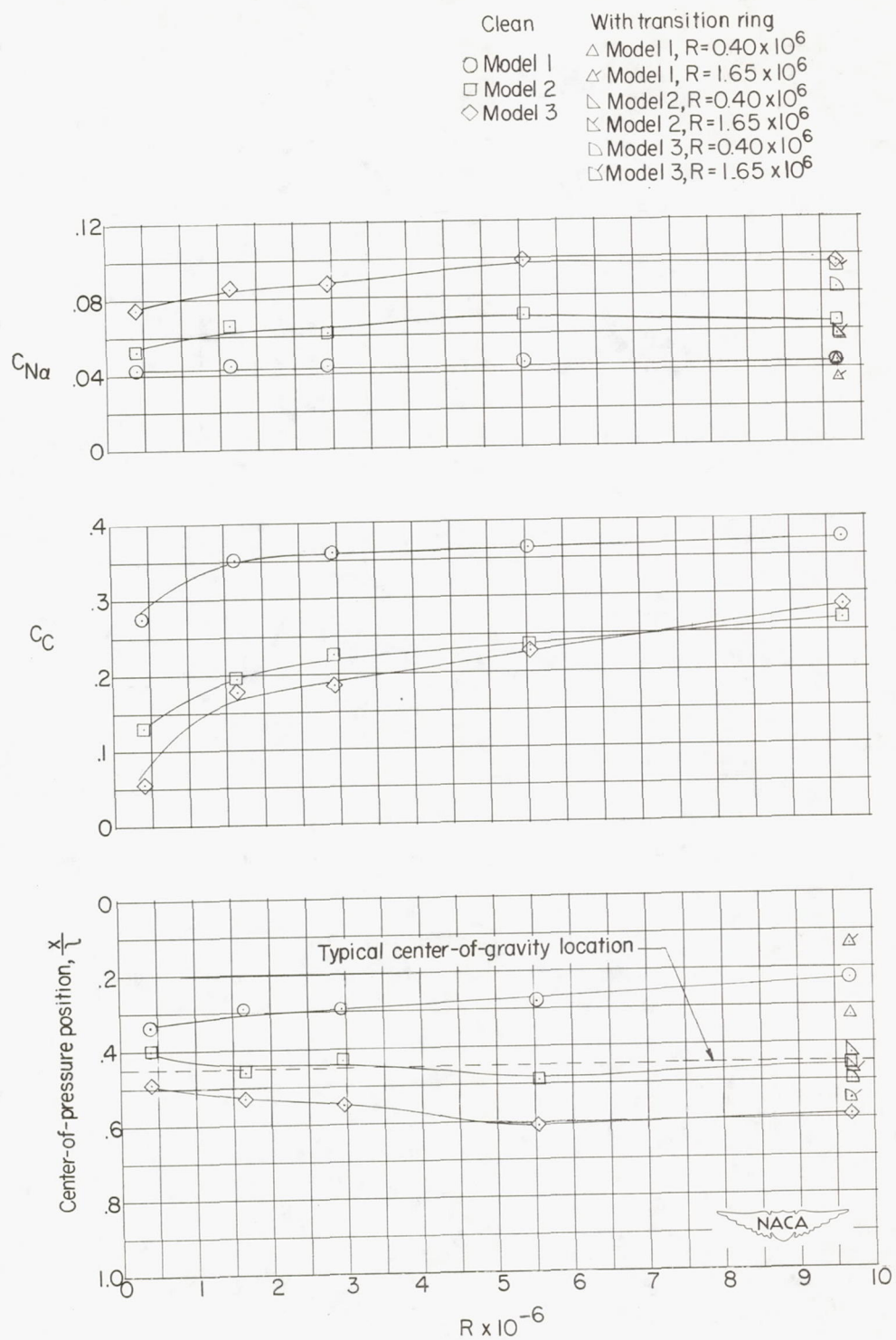
(b) Models 1, 2, and 3.

Figure 13.- Continued.
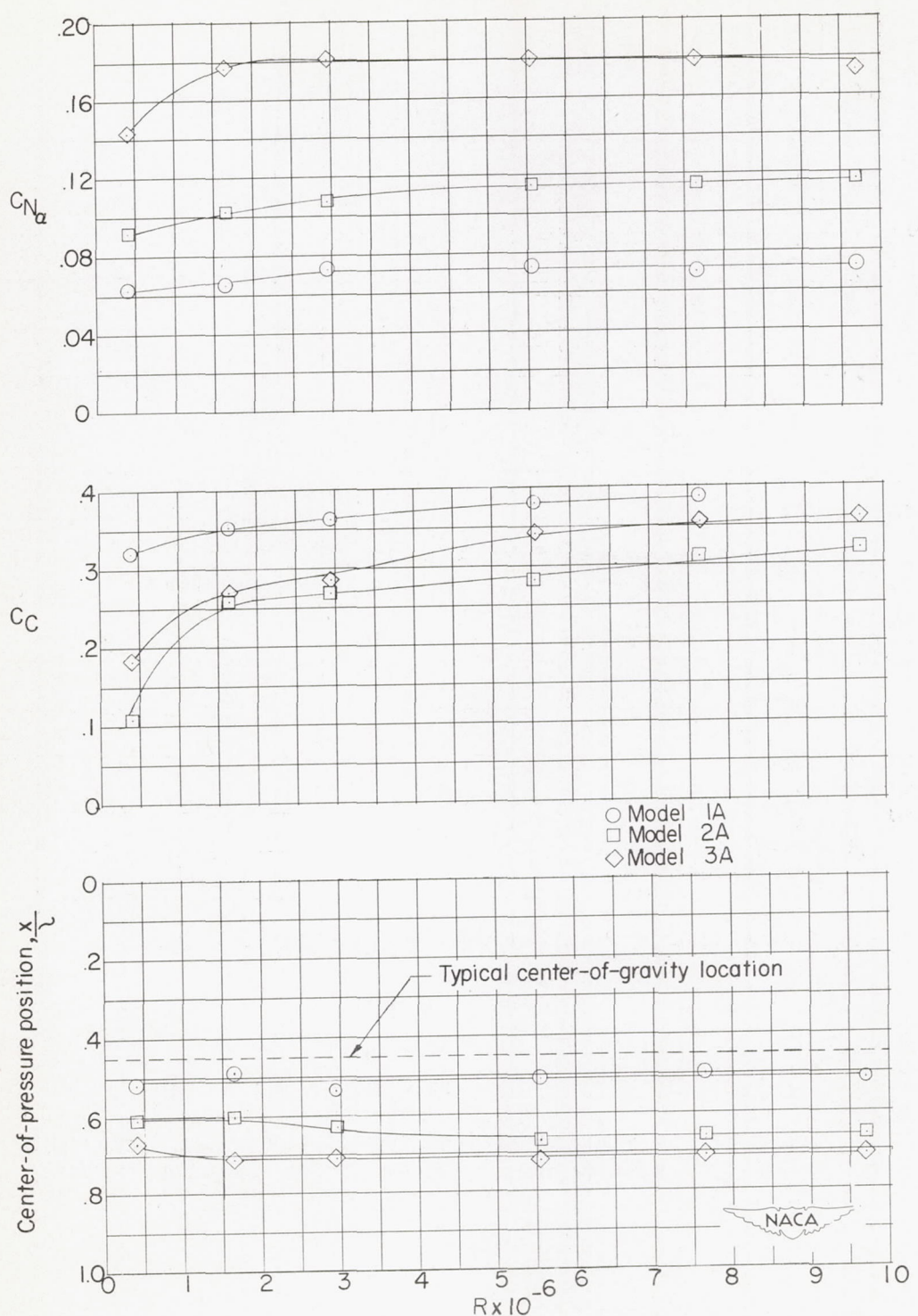
(c) Models 1A, 2A, and 3A.

Figure 13.- Concluded.
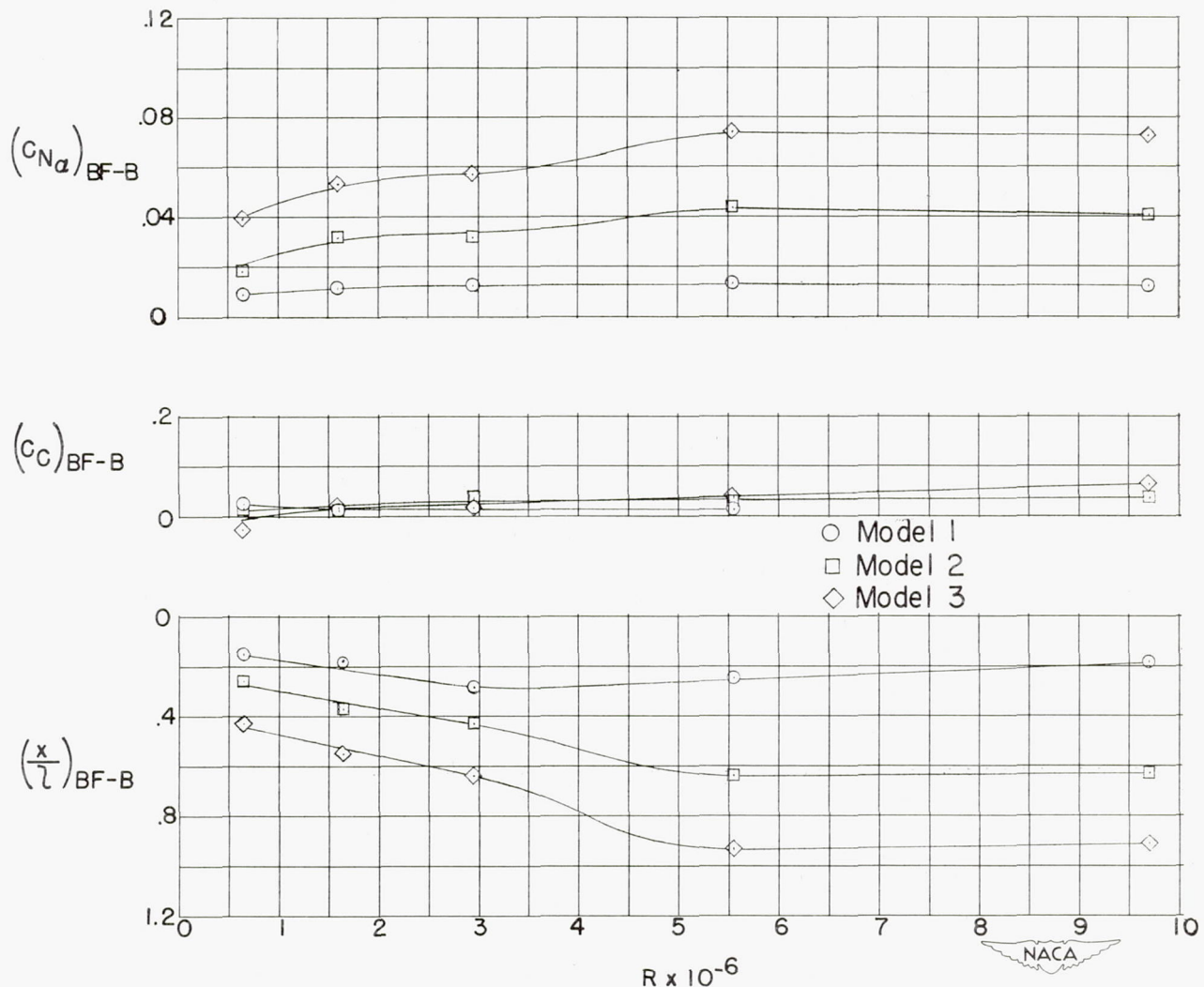
(a) Models 1, 2, and 3.

Figure 14.- Variation of incremental aerodynamic characteristics at
$\alpha = 0^{\circ}$ with Reynolds number (based upon body frontal area).
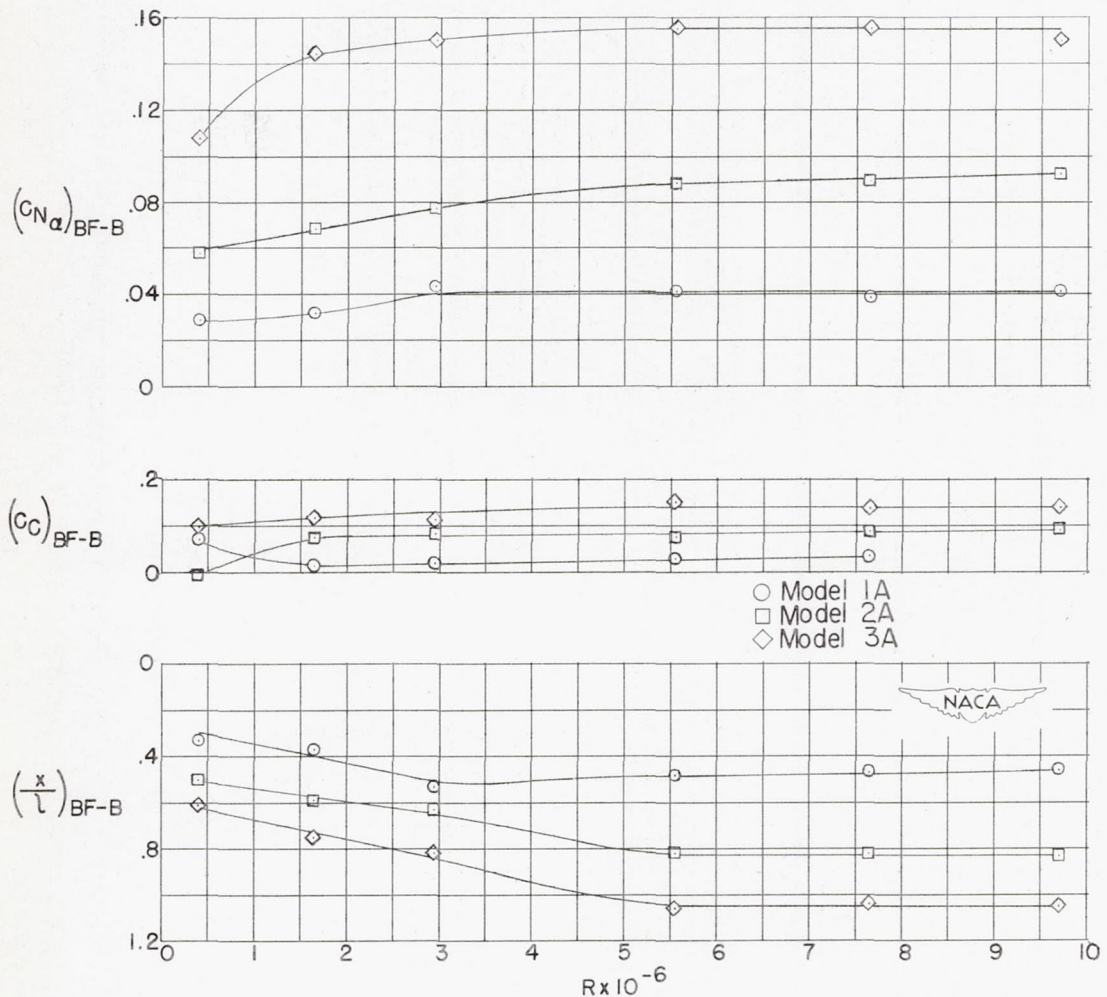
(b) Models 1A, 2A, and 3A.

Figure 14.- Concluded.
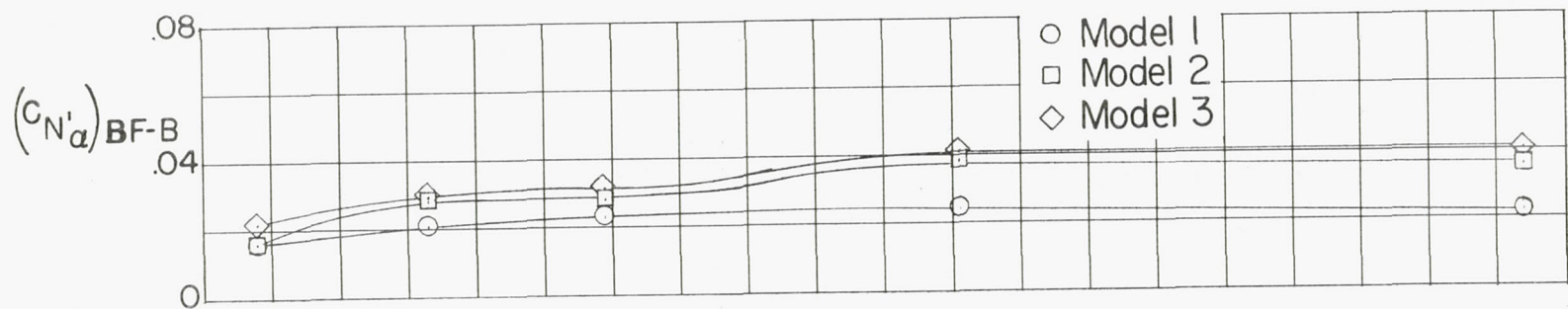
(a) Models 1, 2, and 3.
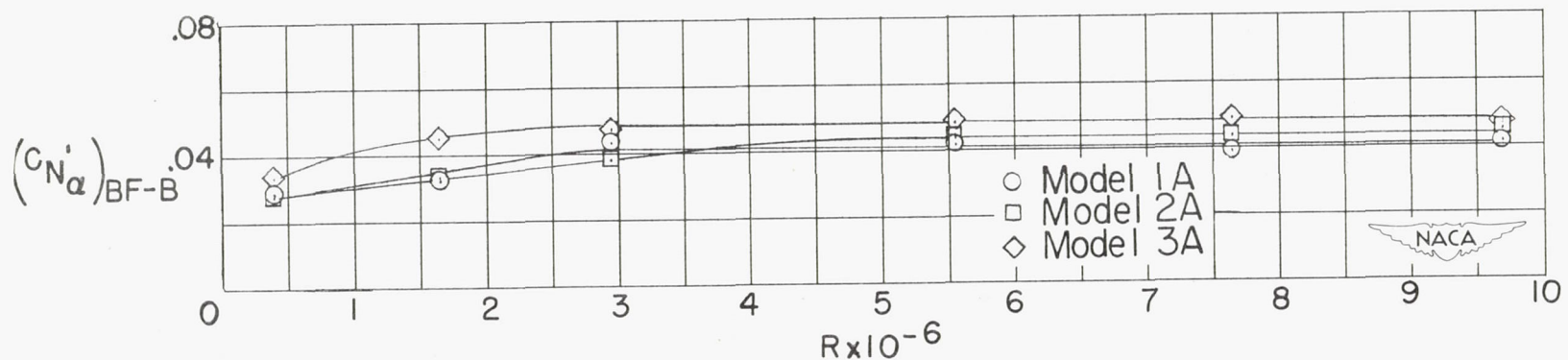
(b) Models 1A, 2A, and 3A.

Figure 15.- Variation of incremental aerodynamic characteristics at $\alpha = 0^{\circ}$ with Reynolds number (based upon exposed plan-form area of two fins).

R = 0.40 x 10⁶   R = 0.40 x 10⁶   R = 0.40 x 10⁶

R = 1.65 x 10⁶   R = 1.65 x 10⁶   R = 1.65 x 10⁶

R = 2.95 x 10⁶   R = 2.95 x 10⁶   R = 2.95 x 10⁶

R = 5.55 x 10⁶   R = 5.55 x 10⁶   R = 5.55 x 10⁶

R = 7.65 x 10⁶   R = 7.65 x 10⁶

R = 9.70 x 10⁶   R = 9.70 x 10⁶

$\alpha = 0°$ $\alpha = 3°$ $\alpha = 6°$
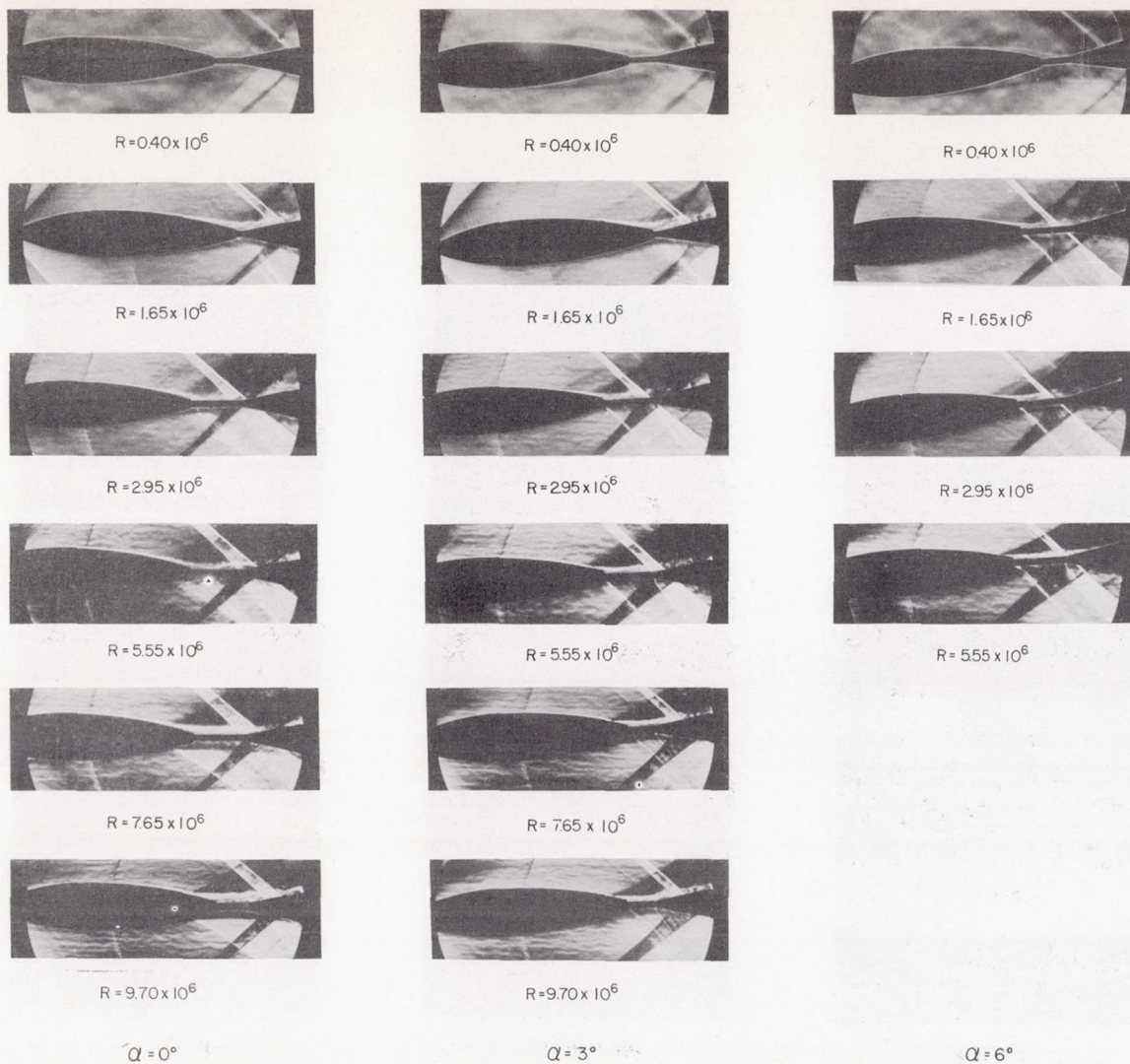
(a) Model 1 (no fins) at $\alpha = 0°$, $3°$, and $6°$.

L-79246

Figure 16.- Schlieren photographs of configurations at various Reynolds numbers.
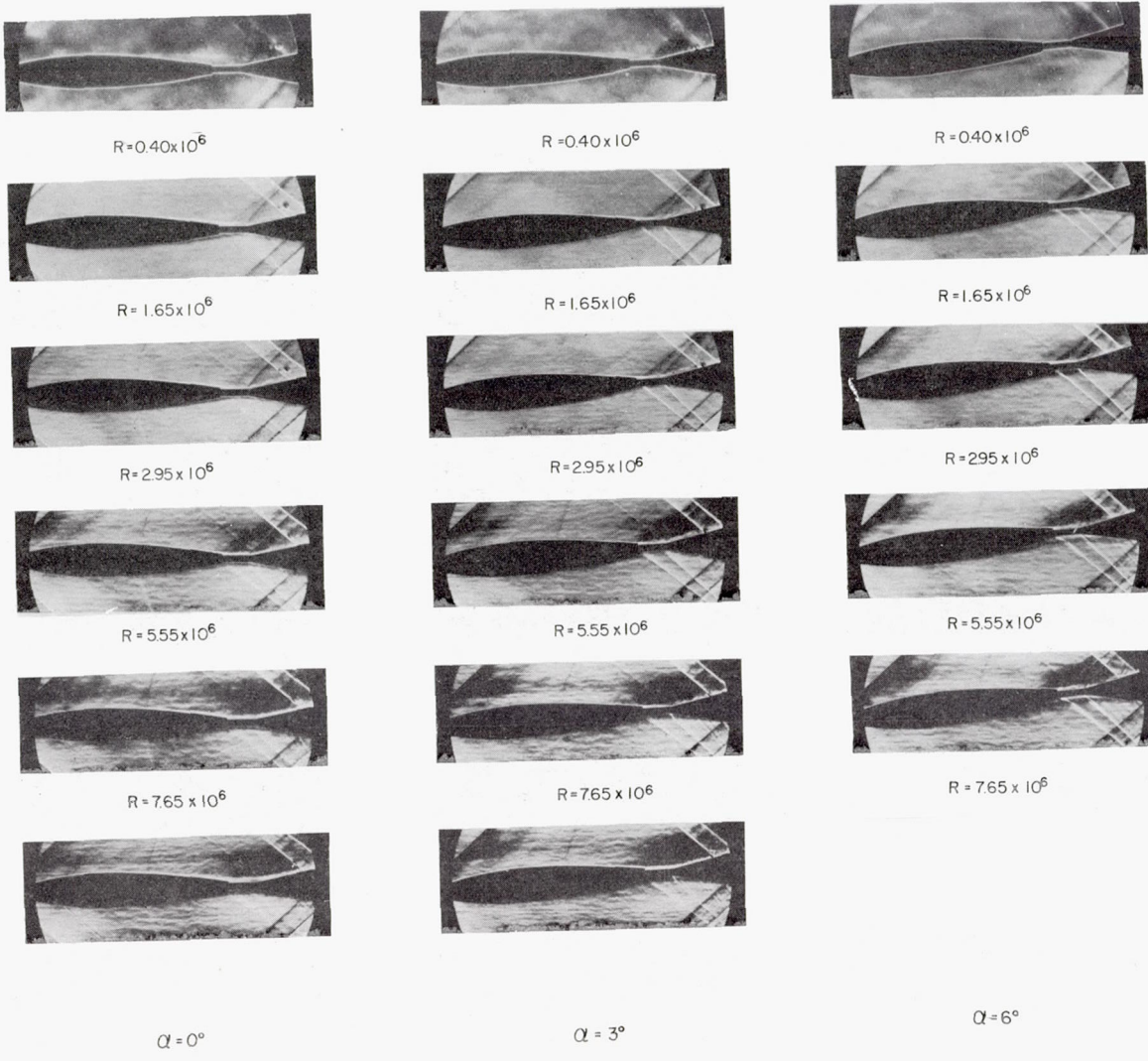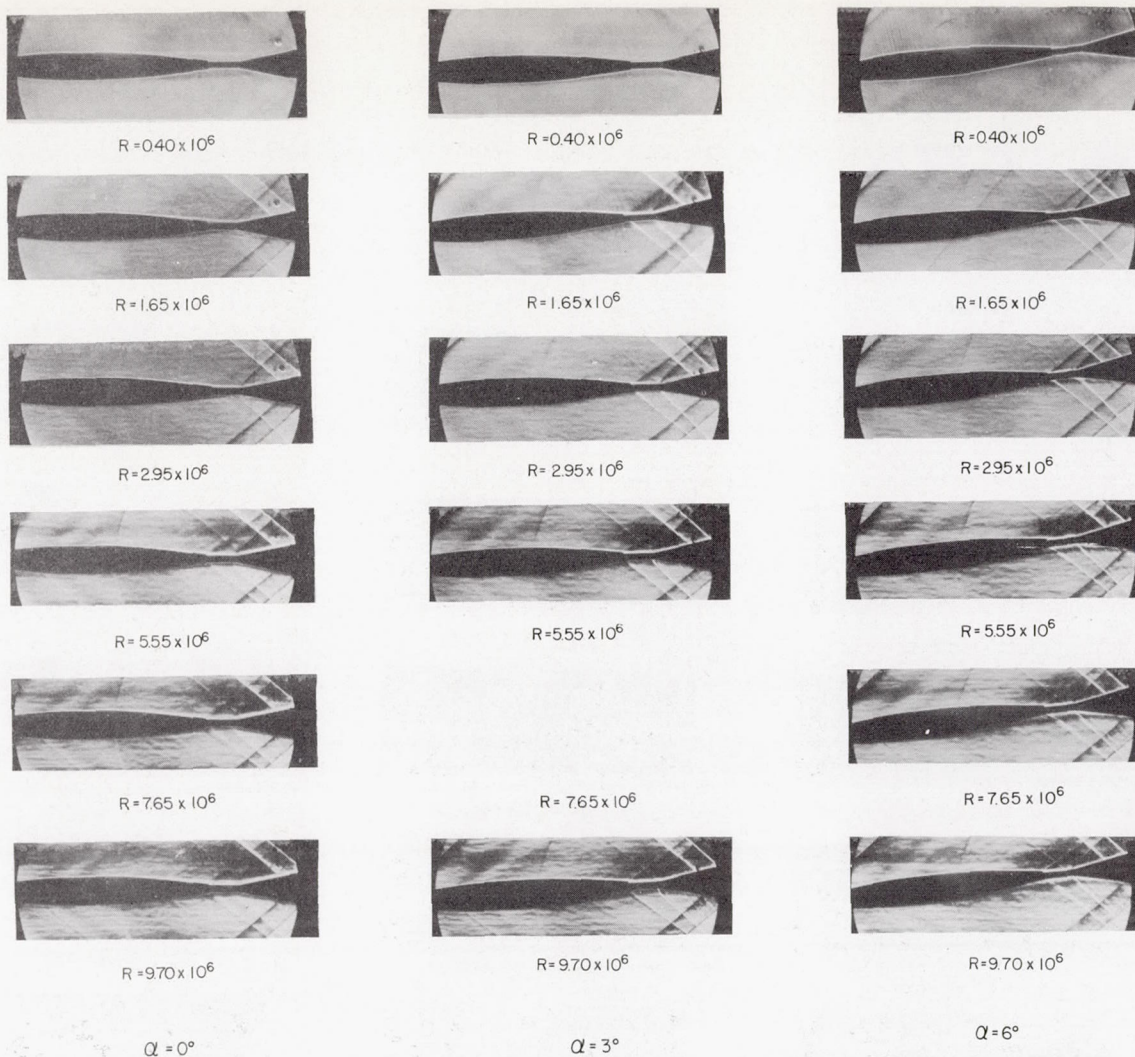
R =0.40x10⁶   R =0.40x10⁶   R =0.40x10⁶

R = 1.65x10⁶   R = 1.65x10⁶   R = 1.65x10⁶

R = 2.95x10⁶   R = 2.95x10⁶   R = 295 x10⁶

R = 5.55 x10⁶   R = 5.55x10⁶   R = 5.55x10⁶

R = 7.65 x 10⁶   R = 7.65 x 10⁶   R = 7.65 x 10⁶

α = 0°   α = 3°   α = 6°

(b) Model 2 (no fins) at α = 0°, 3°, and 6°.

L-79247

Figure 16.- Continued.

R =0.40 x 10⁶   R =0.40 x 10⁶   R =0.40 x 10⁶

R = 1.65 x 10⁶   R = 1.65 x 10⁶   R = 1.65 x 10⁶

R = 2.95 x 10⁶   R = 2.95 x 10⁶   R = 2.95 x 10⁶

R = 5.55 x 10⁶   R = 5.55 x 10⁶   R = 5.55 x 10⁶

R = 7.65 x 10⁶   R = 7.65 x 10⁶   R = 7.65 x 10⁶

R = 9.70 x 10⁶   R = 9.70 x 10⁶   R = 9.70 x 10⁶

α = 0°   α = 3°   α = 6°

(c) Model 3 (no fins) at α = 0°, 3°, and 6°.

L-79248

Figure 16.- Continued.

R=0.40 x 10⁶   R=0.40 x 10⁶   R=0.40 x 10⁶

R=1.65 x 10⁶   R=1.65 x 10⁶   R=1.65 x 10⁶

R=2.95 x 10⁶   R=2.95 x 10⁶   R=2.95 x 10⁶

R = 5.55x 10⁶   R = 5.55x 10⁶   R = 5.55 x 10⁶

R = 9.70x 10⁶   R = 9.70x 10⁶   R=9.70 x 10⁶
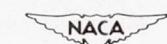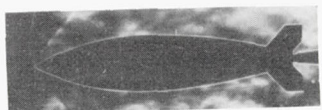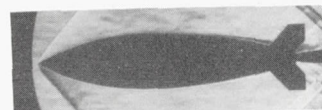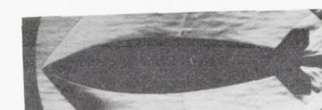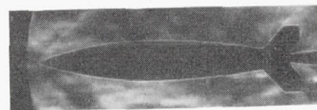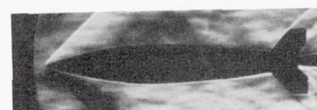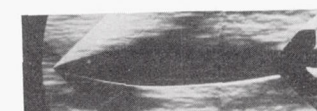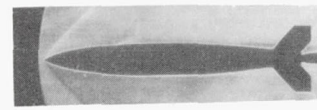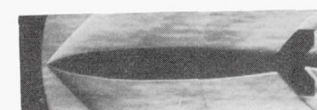
Model 1   Model 2   Model 3

(d) Models 1, 2, and 3 at $\alpha = 0^\circ$.

Figure 16.- Concluded.

L-79249